Structural Engineering and Mechanics, *Vol. 70, No. 1 (2019) 13-31*
DOI: https://doi.org/10.12989/sem.2019.70.1.013

Numerical simulation and analytical assessment of STCC columns filled with UHPC and UHPFRC

Chau V. Nguyen[1a], An H. Le[*2,3] and Duc-Kien Thai[4b]

[1]*Institute of Research and Development, Duy Tan University, 03 Quang Trung, Danang, Vietnam*
[2]*Division of Construction Computation, Institute for Computational Science, Ton Duc Thang University, Ho Chi Minh City, Vietnam*
[3]*Faculty of Civil Engineering, Ton Duc Thang University, Ho Chi Minh City, Vietnam*
[4]*Department of Civil and Environmental Engineering, Sejong University, 98 Gunja-dong, Gwangjin-gu, Seoul, 143-747, South Korea*

(Received October 30, 2018, Revised March 15, 2019, Accepted March 19, 2019)

Abstract. A nonlinear finite element model (FEM) using ATENA-3D software to simulate the axially compressive behavior of circular steel tube confined concrete (CSTCC) columns infilled with ultra high performance concrete (UHPC) was presented in this paper. Some modifications to the material type "CC3DNonlinCementitious2User" of UHPC without and with the incorporation of steel fibers (UHPFRC) in compression and tension were adopted in FEM. The predictions of utimate strength and axial load versus axial strain curves obtained from FEM were in a good agreement with the test results of eighteen tested columns. Based on the results of FEM, the load distribution on the steel tube and the concrete core was derived for each modeled column. Furthermore, the effect of bonding between the steel tube and the concrete core was clarified by the change of friction coefficient in the material type "CC3DInterface" in FEM. The numerical results revealed that the increase in the friction coefficient leads to a greater contribution from the steel tube, a decrease in the ultimate load and an increase in the magnitude of the loss of load capacity. By comparing the results of FEM with experimental results, the appropriate friction coefficient between the steel tube and the concrete core was defined as 0.3 to 0.6. In addition to the numerical evaluation, eighteen analytical models for confined concrete in the literature were used to predict the peak confined strength to assess their suitability. To cope with CSTCC stub and intermediate columns, the equations for estimating the lateral confining stress and the equations for considering the slenderness in the selected models were proposed. It was found that all selected models except for EC2 (2004) gave a very good prediction. Among them, the model of Bing *et al.* (2001) was the best predictor.

Keywords: UHPC; UHPFRC; steel tube; concrete core; FEM; ATENA-3D; confined concrete

1. Introduction

Steel tube confined concrete (STCC) columns is a special type of concrete filled steel tube (CFST) columns where only the concrete core only is loaded (Aboutaha and Machado 1998, An and Fehling 2016a, Yu *et al.* 2010, Han *et al.* 2005). In STCC columns, the steel tube mainly works to provide the confining stress to the concrete core and carries less load, thereby generating much more effective confinement (Han *et al.* 2005, An and Fehing 2017a, b). Accordingly, STCC columns exhibit higher strength and better ductility as compared to the conventional CFST columns with the same dimensions. Previous studies recommended that STCC columns should be used instead of the conventional CFST columns when the columns strength and ductility are considered as the most important design factors (Aboutaha and Machado 1998, Yu *et al.* 2010, Han *et al.* 2005, 2008). Furthermore, the construction of the beam-column joint using STCC columns is easier and faster than those using CFST columns (Liu *et al.* 2009). Among the common cross section shapes introduced in the literature (i.e., square, rectangular, circular, elliptic and octagonal shapes), circular section is found to be the most optimum and to provide the best confinement effect (An and Fehling 2017c, Han *et al.* 2014). A large number of existing experimental studies on the compressive behavior of circular STCC (CSTCC) columns have been recently reported in a review study by An and Fehling (2017b). The majority of previous tests focused on CSTCC columns with the employment of normal strength concrete (NSC) or high strength concrete (HSC) having compressive strength of concrete cylinder smaller than 120 MPa (e.g., Tomii *et al.* 1985, Sakino *et al.* 1985, Orito *et al.* 1987, O'Shea and Bridge 1994, 2000, Johansson 2002, Johansson and Gylltoft 2002, Fam *et al.* 2004, Han *et al.* 2005, 2008, Liu *et al.* 2009, De Oliveira *et al.* 2010, Yu *et al.* 2010, Huang *et al.* 2012), while experimental studies concerning with ultra high performance concrete (UHPC) or ultra high strength concrete (UHSC) having compressive strength of concrete cylinder higher than 120 MPa remain extremely limited. Only two series of tests on this column type using UHPC and UHSC were conducted and reported by the research group led by Professor Tue (Tue *et al.* 2004a, b, Schneider 2006) and another group led by Professor Liew (Liew and Xiong 2010, 2012, 2014, Xiong 2012, Xiong *et al.* 2017),

*Corresponding author, Dr.-Ing.
E-mail: lehoangan@tdtu.edu.vn
[a]Ph.D.
[b]Assisstant Professor

http://www.techno-press.com/journals/sem&subpage=7
ISSN: 1225-4568 (Print), 1598-6217 (Online)

respectively.

It is now widely accepted that UHPC is a material that provides better mechanical properties than NSC and HSC, thus making it an attractive alternative to NSC and HSC in construction (An and Fehling 2017a, b, Fehling *et al.* 2014, Liew and Xiong 2010, Graybeal 2005). It is widely accepted that NSC has concrete strength of cylinder smaller than 60 MPa, while HSC is defined as concrete with concrete strength of cylinder varying between 60 MPa and 90 MPa (Liew and Xiong 2015). Accordingly, ultra high strength concrete (UHSC) has concrete strength of cylinder higher than 90 MPa. This concrete classification is adopted in this study. In addition to the superior mechanical properties such as compressive strength higher than 120 MPa, elastic modulus ranging between 45-60 MPa, usable tensile strength, and enhanced durability, UHPC poses high self-compacting characteristics (An and Fehling 2017d, Graybeal 2005, Ismail *et al.* 2016, Schmidt and Fehling 2005). Therefore, the use of UHPC in CFST or STCC columns results in not only a reduction in member size but also a greater convenience for casting concrete without any additional vibrations. As also indicated in the studies by An and Fehling (2017a, b), CSTCC column is the best choice to eliminate the inherent brittle nature of UHPC which normally associated with very high compressive strength. Moreover, steel fibers reinforced UHPC (UHPFRC) is also an optional solution to enhance the strength and ductility of unconfined UHPC (An and Fehling 2017d). Therefore, the potential benefits of confining UHPC or UHPFRC columns with circular steel tube should be further investigated.

To support the experimental works, some analytical and numerical studies on CSTCC columns have been undertaken. Johansson (2002) carried out a three-dimensional nonlinear finite element model (FEM) to address the influences of bond strength and confinement on the mechanical behavior and the increased compressive strength of CSTCC stub and slender columns infilled with NSC and HSC. Starossek *et al.* (2008) numerically investigated the loading tranfer by natural bonding resistance at mechanical shear connectors at the interface between the steel tube and the concrete core for the CFST columns using NSC subjected to loading on only the concrete core. Likewise, Yu *et al.* (2010) established a FEM with the assistance of ABAQUS software to investigate the mechanism of STCC stub columns using NSC. Haghinejad and Nematzdeh (2016) also performed a FEM in ABAQUS software to carry out a parametric study of the effect of column parameters on the compressive behavior of short CSTCC columns using NSC. Normally, the bond strength is simulated in FEM by using the friction coefficient as an input parameter. Accordingly, Liu *et al.* (2016) investigated the effect of friction in CSTCC stub columns using concrete with compressive strength up to 80 MPa through a FEM established in ABAQUS software. These authors found that the friction coefficient smaller than 0.6 significantly affects the stresses in the steel tube and the ultimate load of the column. The formulae to precisely predict the hoop and longitudinal stresses in the steel tube with taking into account the friction were also proposed in Liu *et al.* (2016). An and Fehling (2016b, 2017e) presented a FEM in ATENA-3D software to verify the tested columns of Schneider (2006) using UHPC, in which they insisted that the steel tube thickness has a major influence on the strength and ductility. A similar FEM accounting for a wide range of concrete strengths (i.e., NSC, HSC and UHPC) varying between 16 MPa and 200 MPa was introduced by An and Fehling (2017f). Ding *et al.* (2017) addressed the composite action in STCC stub columns using NSC through the numerical and theoretical approaches. The friction coefficient between the steel tube and core concrete could be suitably determined by the values ranging between 0.4 and 0.6.

There were many analytical models for confined concrete available in the literature. However, most of these models were developed for the use of NSC and HSC and not applicable to UHSC and UHPC. De Oliveira *et al.* (2010) used the previous confined models of CFST columns to predict the peak confined strength of their tests on CSTCC columns with various slenderness and using concrete up to 105.5 MPa. Recently, Liu *et al.* (2018) have evaluated some existing confined models for predicting the confined concrete strength of CSTCC stub columns using thin steel tube. There has been relatively little attention paid to the evaluation of confined models for higher concrete strength. The availability of confined concrete models for UHPC and UHPFRC in STCC columns is still questionable. Therefore, there is a need to conduct more studies to assess the confined concrete models in the case of UHPC and UHPFRC.

Set against the background as mentioned above, this study is aimed at providing numerical and analytical evaluations of the confined strength in CSTCC columns using UHPC and UHPFRC based on the actual test results. A nonlinear FEM to simulate eighteen tested columns was established in ATENA-3D software. In addition to the material model for the steel tube, some modifications to material type “CC3DNonlinCementitious2User” of UHPC and UHPFRC in compression and tension were made in FEM. In addition to the proposed model for the concrete core in the compression, two different tensile stress-strain models were proposed for UHPC and UHPFRC, based on CEB-FIP Model Code 1990 and Kang and Kim (2011), respectively. The ultimate strengths and the axial load versus axial strain (L-S) curves of all modelled columns obtained from FEM were compared with the test results. Through the results of FEM, the influence of friction coefficient was clarified. Furthermore, the range of friction coefficient was also determined. Finally, a total of eighteen confined concrete models were collected and utilized to predict the peak confined strength of the tested columns. The equation for estimating the lateral confining stress and the equation for considering the slenderness of the columns were proposed in these models. The applicability of the selected models was identified.

2. Summary of tested columns

Tests on CSTCC columns made from UHPC and UHPFRC were performed by An and Fehling (2017g, h).

Table 1 Dimensions and material properties of tested columns

Specimens	V_f (%)	f_c (MPa)	f_t (MPa)	f_y (MPa)	E_c (GPa)	E_s (GPa)	$D\times t$ (mm×mm)	L (mm)	N_u (kN)	f_{cc} (MPa)	ξ
SF0-t50-L600		190.4	8.2	445.9	46.19	197.9	152.4×5.0		3645.94	294.50	0.34
SF0-t63-L600	0	198.0	7.7	373.4	46.94	201.4	152.4×6.3		3692.81	300.65	0.36
SF0-t88-L600		178.9	7.1	392.6	48.37	197.7	152.4×8.8		4200.84	305.24	0.61
SF1-t50-L600		195.6	8.4	445.9	48.69	197.9	152.4×5.0		3997.48	240.70	0.33
SF1-t63-L600	1	195.5	8.2	373.4	47.88	201.4	152.4×6.3	600	3807.97	248.20	0.36
SF1-t88-L600		195.5	7.3	392.6	49.65	197.7	152.4×8.8		4288.54	262.87	0.56
SF2-t50-L600		192.4	8.7	445.9	48.56	197.9	152.4×5.0		4224.02	229.04	0.34
SF2-t63-L600	2	187.8	9.4	373.4	48.58	201.4	152.4×6.3		4033.01	251.13	0.37
SF2-t88-L600		188.2	8.5	392.6	4.842	197.7	152.4×8.8		4354.06	265.36	0.58
SF0-t50-L1000		190.4	8.2	445.9	46.18	197.9	152.4×5.0		3383.35	212.55	0.34
SF0-t63-L1000	0	198.0	7.7	373.4	46.94	201.4	152.4×6.3		3861.14	233.95	0.33
SF0-t88-L1000		178.9	7.1	392.6	48.37	197.7	152.4×8.8		3919.86	251.02	0.61
SF1-t50-L1000		195.6	8.4	445.9	48.69	197.9	152.4×5.0		3724.06	251.67	0.33
SF1-t63-L1000	1	195.5	8.2	373.4	47.88	201.4	152.4×6.3	1000	3535.31	230.43	0.36
SF1-t88-L1000		195.5	7.3	392.6	49.65	197.7	152.4×8.8		4178.66	233.65	0.56
SF2-t50-L1000		192.4	8.7	445.9	48.56	197.9	152.4×5.0		3995.71	274.80	0.34
SF2-t63-L1000	2	187.8	9.4	373.4	48.58	201.4	152.4×6.3		3584.70	292.95	0.37
SF2-t88-L1000		188.2	8.5	392.6	48.42	197.7	152.4×8.8		4099.79	287.42	0.58

The detailed information of eighteen tested specimens is given in Table 1, where V_f is the volume of steel fibers (%), f_c is the unconfined compressive strength of concrete core, f_y is the yield strength of the steel, E_c is the elastic modulus of the concrete core, E_s is the elastic modulus of the steel tube, D is the nominal outer diameter of the steel tube, t is the nominal thickness of the steel tube, L is the length of the steel tube, N_u is the ultimate load measured from the tests. The basic mechanical properties of the steel tube were determined by tensile coupon tests, while the compressive strengths (f_c) of the concrete core were determined from the compression tests on the cylinders of 100 mm×200 mm. Besides, the tensile strengths (f_t) of the concrete core were derived from the direct tension tests on the prisms of 40 mm×40 mm×160 mm. The tested specimens consisted of nine short columns (L = 600 mm) and nine intermediate columns (L = 1000 mm). According to AIJ (2001), the short columns have the ratio of length-to-diamter (L/D) smaller than 4, whereas the intermediate columns are defined as L/D ranging from 4 to 12. The specimens were labeled such that the volume of steel fibers, steel tube thickness and length of the steel tube could be identified from the label. For instance, the specimen "SF1-t6.3-L600" was the column constructed with 1% of steel fibers, nominal steel tube thickness of 6.3 mm and steel tube height of 600 mm. It is noted that the length of the concrete core was about 25 mm smaller than the length of the steel tube at each end (see Fig. 1(a)). Plain UHPC (0% steel fibers) and UHPFRC mixtures with steel fibers at 1% and 2% by volume were cast to fill in 18 hollow steel tube columns. The specimens after casting are depicted in Fig. 1(b). Two steel blocks were produced to apply the concentric load on only the concrete core. Fig. 1(c) described the test setup, and

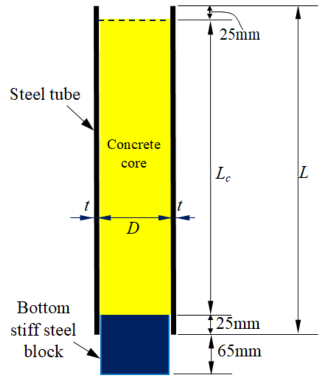

(a) Schematic view of tested columns

(b) Photos of tested columns

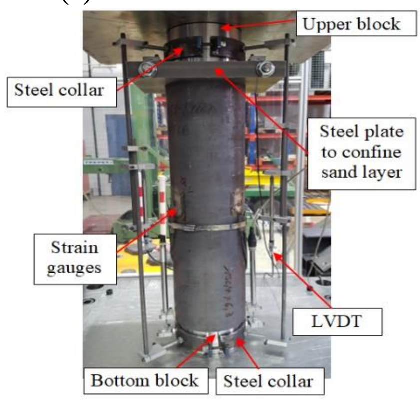

(c) Test setup

Fig. 1 Tested specimens and test setup (An and Fehling 2017 g, h, An *et al.* 2019a, b)

instrumentation, and typical failure mode of tested columns after testing. The experimental ranges of tested parameters for the composite columns were identified as follows:

- Compressive strength of UHPC and UHPFRC: f_c = 178.9 MPa – 198 MPa.
- Steel tube grade: f_y = 373.4 MPa – 445.9 MPa.
- Tube diameter to wall thickness ratio: D/t = 17.31 – 30.48.
- Column slenderness ratio: L_c/D = 3.94 – 6.56.
- Steel fiber volume: V_f = 0, 1, and 2%.
- Confinement index ξ : ξ = 0.33 – 0.61

where the confinement index ξ was defined as

$$\xi = \frac{f_y \cdot A_s}{f_c \cdot A_c} \tag{1}$$

in which A_s and A_c are the cross-sectional area of the steel section and the concrete section, respectively. L_c is the length of the concrete core

The compressive behavior of the tested columns can be briefly described as follows:

(1) The general compressive behavior including the load versus strain curve, and the failure pattern of the short columns was similar to that of the intermediate columns.

(2) The incorporation of steel fibers has insignificant effect on the strength and ductility.

(3) The steel tube thickness has significant effect on the strength and ductility.

(4) The strength and ductility were significantly enhanced with increasing the confinement index ξ.

(5) When the ratio of *L/D* increased, the ultimate strength was increased, while the ductility of the columns was decreased.

3. Numerical assessment

To perform numerical simulations of eighteen tested specimens, a nonlinear FEM was constructed using a specialized software package, ATENA-3D. To facilitate the investigation on the behavior of CSTCC columns, the established FEM is able to simulate these columns in a realistic way, such the nonlinear behavior of the steel tube and the confined concrete, the bond between two materials and the increase in the column strength due to the confining effect were taken into consideration. Due to the symmetryy of the circular specimens and the concentric load which is applied in the same way at both ends of the columns, only one fourth of each specimen as seen in Fig. 2 was modelled to save time for the analysis progress.

3.1 Finite element type and mesh

The components of one modelled column including the steel tube, the concrete core and the loading plates were defined as individual bodies in order to simulate the bond between them. It should be mentioned that the loading plates were modelled as two stiff steel plates at each end surface of the concrete core to ensure that the load is only applied on the concrete section. Due to the limitation of the element type in the library of ATENA-3D, only 3D Solid Tetrahedral Elements which are designated by "CCIsoTetra" with reduced integration (4 nodes) were chosen for modeling the steel tube, the concrete core and the loading plates (Cervenka *et al.* 2013). The size of the mesh was also chosen to reduce the time for computation process and to provide the most accurate results. Moreover, the use of large element sizes results in difficulty to ensure the accuracy of the simulation, whereas small size element sizes consume high amount of analysis time and the convergence difficulty. For this reason, mesh sensitivity analysis was conducted with several mesh sizes including 15, 20, 25, 30 and 35 mm. It was shown from the results of this analysis that there was no significant change in the results when the mesh size was smaller than 25 mm, however the run time for analysis was much increased. Therefore, the global element size was determined to be 25 mm for the steel tube, the concrete core and the loading plates. It should be noted that due to the mesh compatibility requested on the contact surfaces between the steel tube and the concrete core, the concrete core and the loading plates, three components of the specimens should be modelled in the same mesh size. The contact surfaces between the steel tube and the concrete core were simulated using the interface elements which are designated by "CCIsoGap" in ATENA-3D (Cervenka *et al.* 2013). These interface elements were automatically created between two components and assigned by a material type "CC3DInterface" which can precisely describe the bonding behavior between two materials of these two components. Fig. 2 depicted the element type and mesh of the modelled column.

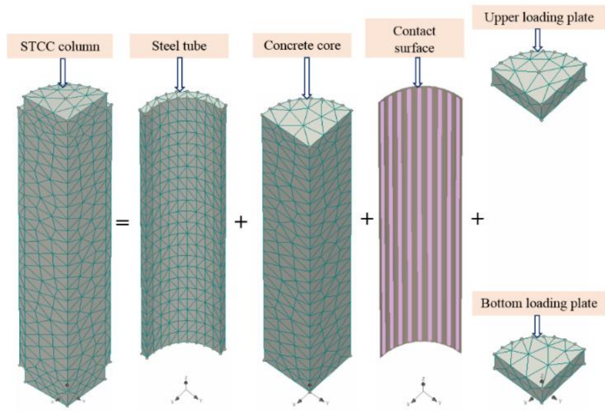

Fig. 2 Modelling of the components of the specimens

It could be seen that the failure mode and compressive behavior of the short columns were similar to the intermediate columns. According to Tao *et al.* (2013), for CFST short columns, the effects of initial imperfections and residual stresses were observed to be minimised by concrete filling and ignored in FEM. This conclusion can be confirmed by the previous numerical studies by Hassanein and Patel (2018), Tao *et al.* (2009), Johansson (2002). Moreover, for STCC short and intermediate columns, the compressive behavior and the lateral deformation of the steel tube depend on the concrete expansion and its failure pattern. Deriving from the mentioned reasons, the effect of initial imperfections and residual stresses were not considered in FEM in this study.

3.2 Loading application and boundary conditions

As seen in the test setup, for the loading application on the test specimens, two circular steel blocks were placed at both ends of the concrete core to minimize the effect of end conditions and to ensure that the applied load transfers to only the concrete section. Therefore, in FEM, the axial load was applied through the stiff steel plates which were modelled at each end surface of the concrete core. A static uniform load was applied to the monitoring point 1 which was placed at the center of the top surface of the upper steel plates. This method of loading application was used to equally transfer the load from the steel plate to the concrete core. Accordingly, all the nodes at the top surface of the

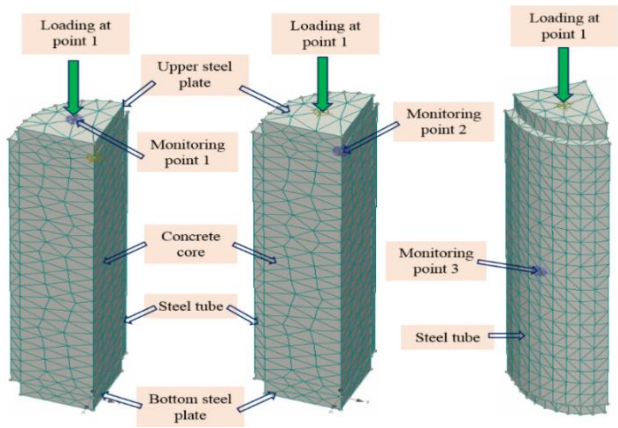

Fig. 3 Loading application and monitoring points

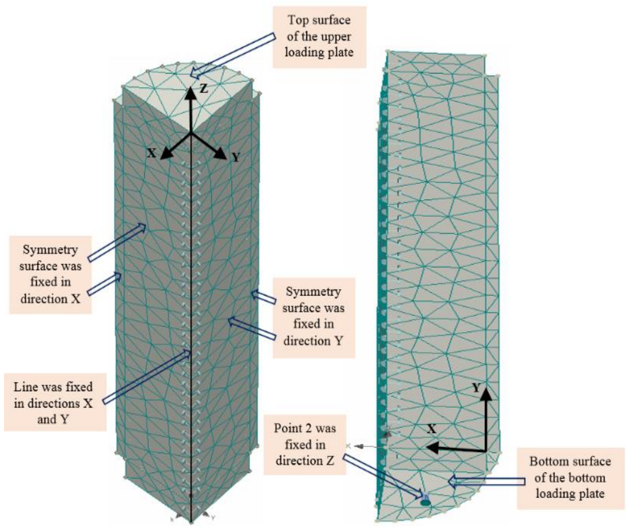

Fig. 4 Boundary conditions

concrete section were forced to have the same vertical displacement, thereby ensuring the concentric loading. The load was measured as the total reaction acting on this monitoring point. In order to capture the post-peak response of the column, the load was applied as an increased deformation at the point 1 of the upper steel plate. The Newton-Raphson iteration method was used to solve the equilibrium of the nonlinear equations for each load increment (Cervenka *et al.* 2013). Due to the fact that only one fourth of the column was modelled, the boundary conditions at the symmetry surfaces and the central axis were chosen to ensure the effect of continuity. All the symmetry planes perpendicular to the X-axis were fixed against the displacement in the X direction, while the displacement in the Y direction was forced to be zero for all the symmetry plane perpendicular to the Y-axis. In addition, the central line of the column was restricted along the X and Y direction. A point 2 coinciding with the central point at the bottom surface of the bottom steel plate was created and fixed in the Z direction. The boundary condition at the point 2 ensures the same loading distribution at both end surfaces of the concrete core.

Three monitoring points (1, 2, 3) were created as shown in Fig. 3, in which the second monitoring point (2) was used

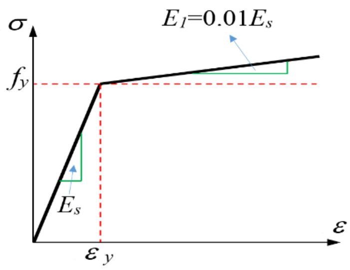

Fig. 5 Stress-strain curve for steel tube

to record the vertical displacements of the concrete core at each step of loading increment and then the vertical strains of the concrete core were derived by the ratio of these displacements to the concrete core length. Furthermore, the third monitoring point (3) created at the center of the outer surface of the steel tube was used to capture the stress and the strain of the steel tube. Fig. 3 describes the loading application and the position of three monitoring points, while Fig. 4 depicts the boundary condition.

3.3 Material models

3.3.1 Stiff steel plates

The material type of the stiff steel plates placed at both end surfaces of the concrete core was defined as 3D Elastic Isotropic material (CC3D ElastIsotropic) (Cervenka *et al.* 2013) with an extremely large elastic modulus of 2.10^6 MPa and the Poisson's ratio of 0.3 in the elastic phase. A very high stiffness for the loading plates was induced by such very high elastic modulus, thereby restricting bending moments in the loading plates under prescribed deformation.

3.3.2 Steel tube

There are a number of stress-strain models of steel tube available in the literature such as elastic-perfectly plastic model, and elastic-plastic model with linear hardening, or multi-linear hardening (Tao *et al.* 2013, Thai *et al.* 2014). It was concluded by Tao *et al.* (2013) that the effects of using three types of stress-strain models on the ultimate strength and the behavior of composite columns can be negligible. In the FEM of this study, an elastic-plastic model with linear hardening as shown in Fig. 5 with the Von-Mises yield criterion were adopted to describe the constitutive behavior of the steel tube. The Von-Mises yield criterion was used due to the biaxial stress state of steel tube in yield condition. In ATENA-3D, the material type "CC3DbilinearSteelVonMises" was used to simulate the behavior of the steel tube (Cervenka *et al.* 2013). To define input parameters for this material type, the average tensile strength f_y and modulus of elasticity E_s were obtained from the tensile coupon tests of steel tubes. Besides, the Poisson's ratio of the steel tube in the elastic part was set to be 0.3, this value has been widely used in the numerical simulation of the steel tube. The strain hardening modulus E_1 was taken as $0.01E_s$.

3.3.3 Concrete core

The material type "CC3DNonlinCementitious2User"

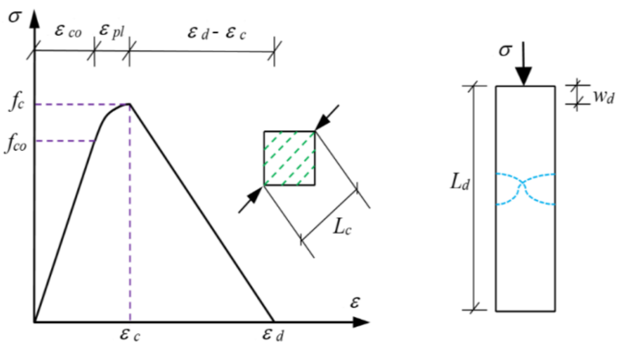

Fig. 6 Compressive stress-strain curve for the concrete core

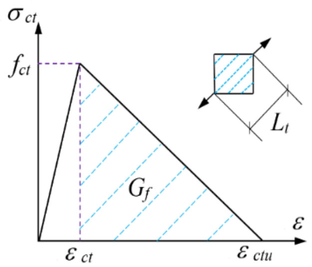

(a) Complete stress-strain curve in tension

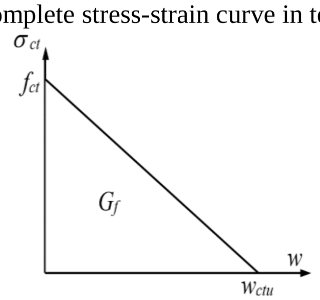

(b) Linear crack opening in tension

Fig. 7 Tensile stress-strain curve for the UHPC without steel fibers

provided in the material library of ATENA-3D (Cervenka *et al.* 2013) was used for modeling the behavior of the concrete core, in which the strength and ductility enhancement due to the confinement effect were taken into account. The principal description of material type and other laws for the concrete core, and the consideration of the confinement effect were explained in detail in the previous study conducted by An and Fehling (2017f). In this section, only the tension and compression laws were developed and presented.

To simulate the compressive behavior of the UHPC and UHPFRC core in the material type "CC3DNonlinCementitious2User", a compressive stress-strain curve was proposed as shown in Fig. 6. The ascending part was modelled as linear elastic up to a compressive strength f_{co}, which was taken as 80% of the peak stress ($f_{co} = 0.8f_c$) according to Fehling *et al.* (2014). The Poisson's ratio in the elastic part was set to be 0.2, this value can be accepted for UHPC and UHPFRC. The hardening part up to the peak stress f_c was defined using the plastic strain ε_{pl}, which can be calculated using Eq. (3). The values of E_c and f_c was taken from the compression test results of cylinders for each batch of the concrete, while the

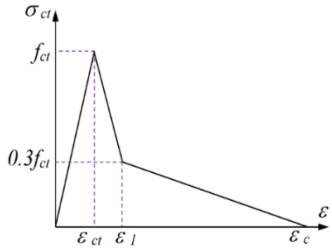

(a) Complete stress-strain curve in tension

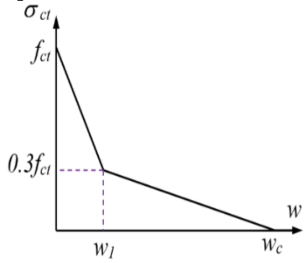

(b) Bilinear crack opening in tension

Fig. 8 Tensile stress-strain curve for the UHPFRC with steel fibers

Eq. (2) proposed by An and Fehling (2017d) can be used for determining the values of the strain ε_c at the peak stress f_c.

$$\varepsilon_c = 0.0257 \cdot f_c^{0.96} \tag{2}$$

$$\varepsilon_{pl} = \varepsilon_c - \varepsilon_{co} = \varepsilon_c - \frac{f_c}{E_c} \tag{3}$$

The descending part was assumed to be linear up to zero stress. In order to capture the increase in the ductility due to the confinement effect in a reasonable way, the inelastic strain ε_d at the zero stress can be computed from the empirical equation proposed by Lim and Ozbakkaloglu (2015)

$$\varepsilon_d = 0.02\, f_c^{0.5} \left(\frac{f_{cc} - f_c}{f_{cc} - f_r} \right) \tag{4}$$

in which, f_r is the residual stress in the stress-strain curve of the tested columns. The residual stress corresponds to the second peak load in the load-strain curve of the tested columns.

With respect to the tension function including post cracking softening behavior in the material type "CC3DNonlinCementitious2User", two different tensile stress-strain curves were proposed for UHPC and UHPFRC as depicted in Figs. 7-8. The softening models of the tensile stress-strain curves were assumed to be linear and bilinear for UHPC and UHPFRC, respectively. For UHPC without steel fibers, the input parameters for the tension function in ATENA-3D including the matrix tensile strength f_{ct}, the corresponding strain ε_{ct} at f_{ct}, the strain ε_{ctu} at the zero stress, the fracture energy G_f, the crack opening w_{ctu} can be determined following Eqs. (5)-(9) in the study by An and Fehling (2017e)

$$f_{ct} = 0.3 \cdot (f_c)^{2/3} \tag{5}$$

$$\varepsilon_{ct} = \frac{f_{ct}}{E_c} \tag{6}$$

$$\varepsilon_{ctu} = \frac{w_{ctu}}{L_t} \tag{7}$$

$$G_f = 73 \cdot f_c^{0.18} \tag{8}$$

$$w_{ctu} = \frac{2 \cdot G_f}{f_{ct}} \tag{9}$$

The parameters for the ascending branch of tensile stress-strain curve for UHPFRC are similar to those of UHPC without steel fibers. However, the bilinear softening curve proposed by Kang and Kim (2011) was adopted to express the post-cracking behavior of UHPFRC. It is mentioned that this proposed model was based on CEB-FIP Model Code 1990 (CEB 1993) for the concrete using a very small size of coarse aggregate. The following equations taken from study by Kang and Kim (2011) were applied for the bilinear softening curve of the matrix of UHPFRC

$$\sigma_{ct} = f_{ct}\left(1 - 0.7\frac{w}{w_c}\right) \quad \text{for} \quad 0.3 f_{ct} \le \sigma_{ct} \le f_{ct} \tag{10}$$

$$\sigma_{ct} = \frac{0.3 f_{ct}}{w_c - w_1}\left(w_c - w\right) \text{for} \quad 0 \le \sigma_{ct} \le 0.3 f_{ct} \tag{11}$$

where w_1 = 0.2 mm and w_c = 0.5 mm

3.3.4 Interaction between the concrete core and the steel tube

The material type "CC3DInterface" in ATENA-3D (Cervenka *et al.* 2013) was adopted to simulate the interface between the concrete core and the steel tube. The detail of this material type can be found in the studies by An and Fehling (2017e, f). The master and slave surfaces were automatically defined by ATENA-3D for the concrete core and the steel tube to reduce the numerical errors. Normally, the slave surface is assigned to a softer material and it has a finer mesh than the master one. The interface elements comprise two matching contact surfaces of the steel tube and the concrete core. These two surfaces can be separated under the influence of the tensile force, however they are not allowed to penetrate into each other in compression. The general bond action between the concrete core and the steel tube was simulated through the Coulomb friction model with a friction coefficient μ. According to many previous studies (e.g., Liu *et al.* 2016, Johansson 2002), the compressive behavior of circular STCC columns is sensitive to the selection of the friction between the steel tube and the concrete core. Because there were no push out tests or other tests to determine the friction between UHPC or UHPFRC and the steel tube, different friction coefficients ranging from 0 to 0.6 were investigated in FEM for each column to perform the sensitivity study. The selected range of the friction coefficients in FEM is based on the suggestions of Baltay and Gjelsvik (1990), Rabbat and Russel (1985), and Aly *et al.* (2010). The value of friction coefficient between the concrete core and the steel tube varies between 0.2 and 0.65 and depends on the type and the surface of the steel tube. This selection accords with the study by Liu *et al.* (2016), in which these authors stated that for circular STCC columns, the friction coefficient smaller than 0.6 causes a significant influence on the stress state of the steel tube and the ultimate load of the columns, while there is no such notable influence with the friction coefficient higher than 0.6. The friction coefficient μ=0 indicates that there is no bonding between two materials. The established FEM in ATENA-3D also studied this case with the purpose of comparing the behavior of the modelled columns between two cases: with bonding and without bonding.

3.4 Comparison of FEM results with experimental results

The accuracy of established FEM in ATENA-3D was validated through comparing the axial load versus strain (L-S) curves and the ultimate loads predicted by the numerical method described above against the experimental results. A total of eighteen tested specimens in this study with the dimensions and the material properties as shown in Table 1 were adopted for modelling and comparisons. Six friction coefficients μ = 0.0, 0.1, 0.2, 0.3, 0.4, 0.5, and 0.6 were used for each modelled column in order to find the most suitable friction coefficient for the corresponding tested column.

Figs. 9-11 present the comparisons between the L-S curves obtained from the FEM and those measured in the experiments. It is evident from these figures that the L-S curves significantly vary with the friction coefficient each time adopted. The results obtained from the FEM indicated that the modelled column using smaller friction coefficient exhibited a smaller initial stiffness, and a higher ultimate load and a better ductility of the post-peak range in comparison with that using higher one. For the short columns in the FEM, the L-S curves presented a strain hardening stage after the elastic stage, and then followed by a stabilized stage which was marked by a slight recovery of load. It was noticed that there was a drop of load before starting a stabilized stage for the modelled columns with steel thickness of t = 6.3 mm and 5.0 mm, while in the case of the modelled columns with t = 8.8 mm, the drop of load did not occur for μ = 0.0 and μ = 0.1. The magnitude of the loss of load capacity in FEM increases with increasing the values of μ. Similar trends in the L-S curves were also observed for the intermediate columns in the FEM, however there were a drop of load for all columns. In the FEM, the short columns performed a more significant recovery of load than the intermediate columns.

From six L-S curves corresponding to six friction coefficients obtained from the FEM, the best suitable friction coefficient for each tested column was selected and given in Table 2 to ensure that the FEM results were in the best agreement with the test results. By comparing the L-S curves with the selected friction coefficient between the FEM results and the test results, it can be seen that the

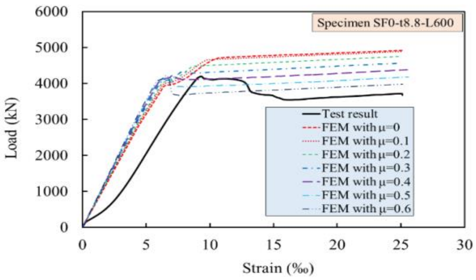

(a) L-S curves of specimen SF0-t8.8-L600

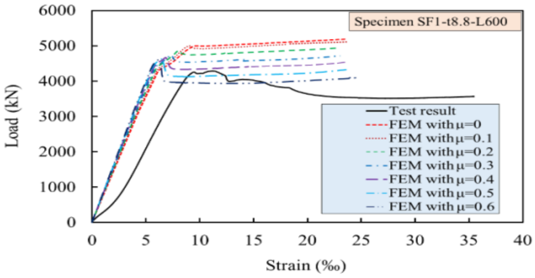

(b) L-S curves of specimen SF1-t8.8-L600

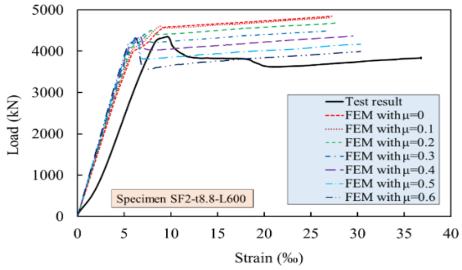

(c) L-S curves of specimen SF2-t8.8-L600

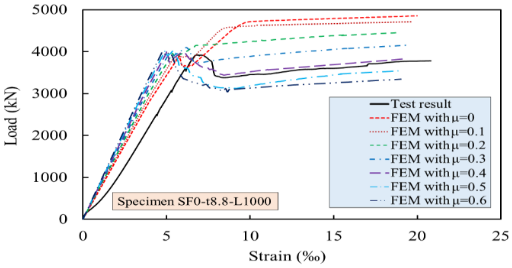

(d) L-S curves of specimen SF0-t8.8-L1000

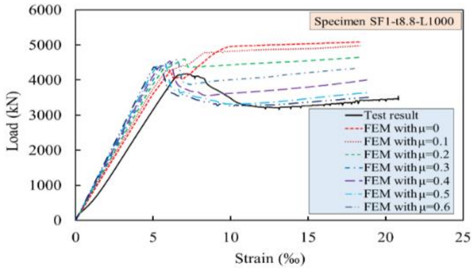

(e) L-S curves of specimen SF1-t8.8-L1000

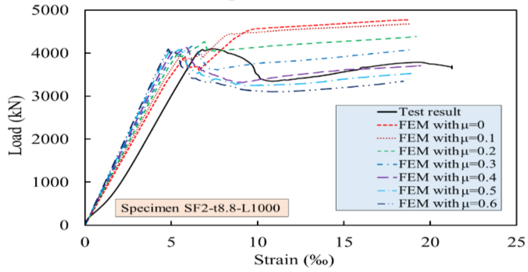

(f) L-S curves of specimen SF2-t8.8-L1000

Fig. 9 FEM results of short columns with t = 8.8 mm

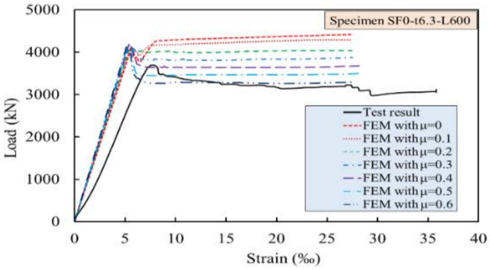

(a) L-S curves of specimen SF0-t6.3-L600

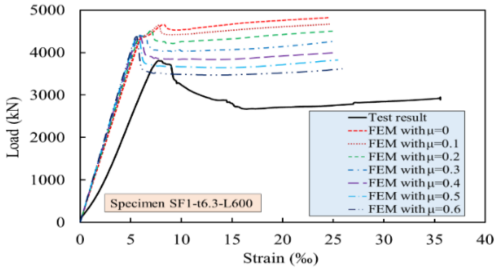

(b) L-S curves of specimen SF1-t6.3-L600

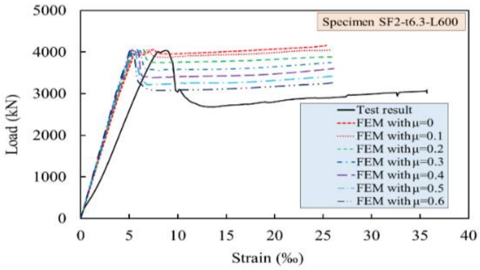

(c) L-S curves of specimen SF2-t6.3-L600

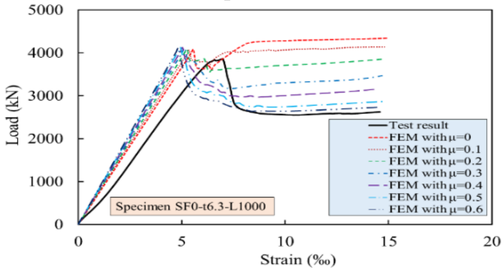

(d) L-S curves of specimen SF0-t6.3-L1000

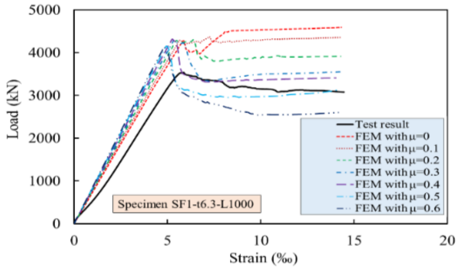

(e) L-S curves of specimen SF0-t6.3-L1000

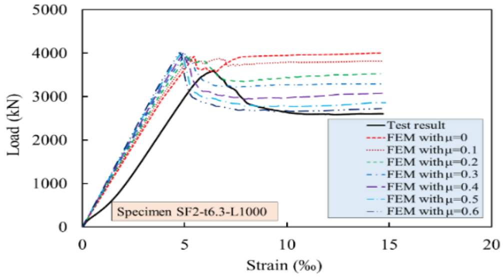

(f) L-S curves of specimen SF2-t6.3-L1000

Fig. 10 FEM results of short columns with t = 6.3 mm

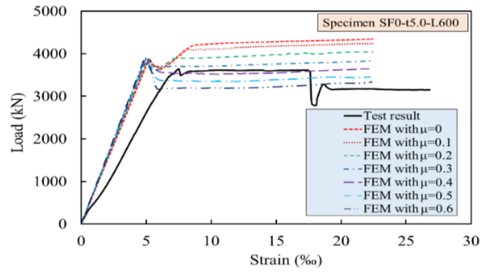

(a) L-S curves of specimen SF0-t5.0-L600

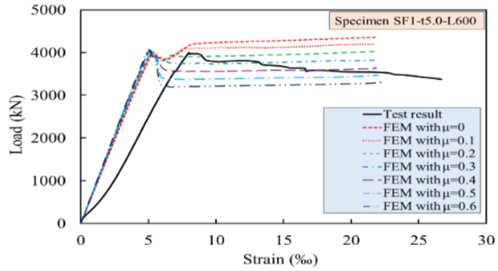

(b) L-S curves of specimen SF1-t5.0-L600

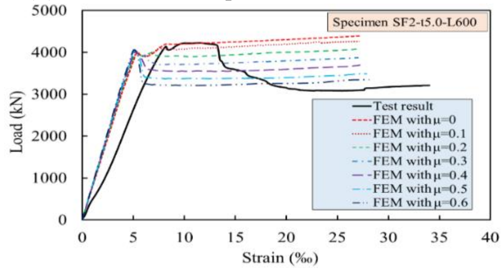

(c) L-S curves of specimen SF2-t5.0-L600

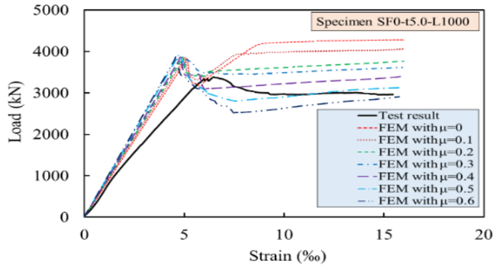

(d) L-S curves of specimen SF0-t5.0-L1000

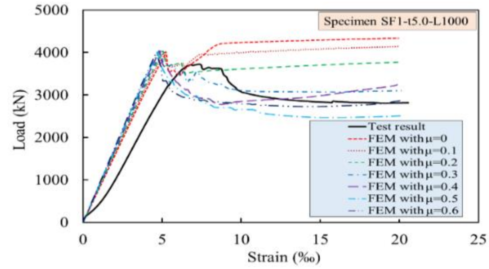

(e) L-S curves of specimen SF1-t5.0-L1000

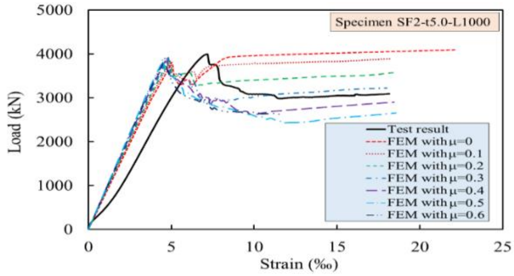

(f) L-S curves of specimen SF2-t5.0-L1000

Fig. 11 FEM results of short columns with t = 5.0 mm

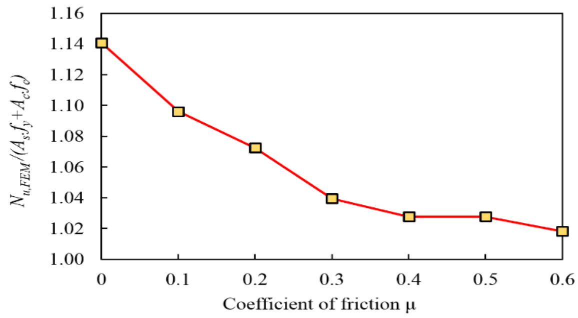

(a) Short column SF2-t8.8-L600

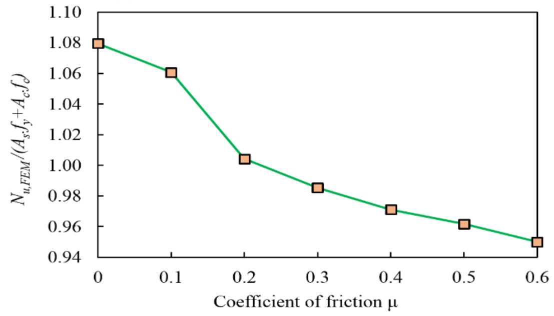

(b) Intermediate column SF2-t8.8-L1000

Fig. 12 Influence of friction coefficient on the ultimate loads (Results obtained from FEM)

numerical curves agree reasonably with the experimental curves, especially for the ultimate load and the trend of the ascending and descending parts. Both numerical and experimental curves display four different parts, comprising an elastic stage, elasto-plastic stage, loss of load capacity stage and stabilized stage. Nevertheless, the numerical curves performed an initial stiffness higher than the experimental curves, leading to the differences in the ascending branch and the axial strain. The main causes for this difference may be attributed to: (1) the slippage between the concrete core and the steel tube within the initial loading as explained in An and Fehing (2017h), (2) the existence of initial imperfection and residual stresses in the steel tube, (3) the use of the thin sand layer for capping.

In Table 2, the ultimate loads predicted by FEM ($N_{u,FEM}$) were compared with those measured from the tests ($N_{u,test}$) through the ratios of $N_{u,FEM}/N_{u,test}$. A mean ratio $N_{u,FEM}/N_{u,test}$ of 1.061 was obtained with a COV of 0.068, indicating that the FEM provides a slight overestimation (6.1%) but with a reasonable accuracy. From Table 2, the appropriate friction coefficient between the steel tube and the concrete core can be defined as 0.3 to 0.6. This result accords with the previous study by Ding *et al.* (2017).

3.5 Effect of the friction coefficient

It is agreed that the change of friction coefficient greatly affects to the ultimate load of CSTCC columns (Liu *et al.* 2016). Fig. 12 shows the influence of the friction coefficient on the ultimate load for the modeled columns SF2-t8.8-L600 and SF2-t8.8-L1000. It should be noted that the remaining modelled columns had the same behavior. In Fig. 12, for the convenience of quantifying the increased strength due to the confinement effect, the ultimate load is

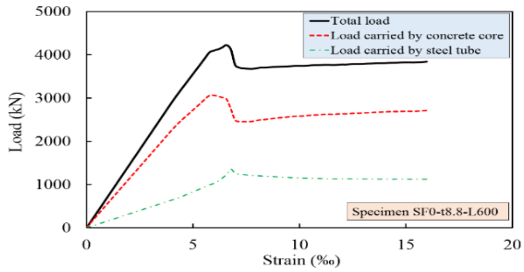

(a) Load distribution of specimen SF0-t8.8-L600 (μ=0.6)

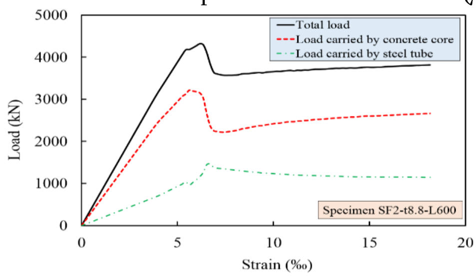

(b) Load distribution of specimen SF2-t8.8-L600 (μ=0.6)

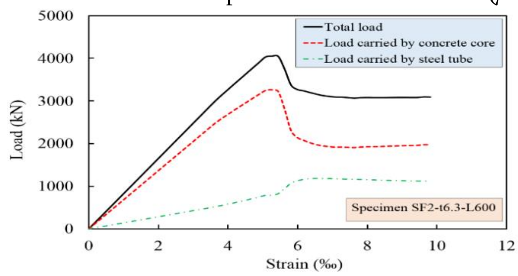

(c) Load distribution of specimen SF2-t6.3-L600 (μ=0.6)

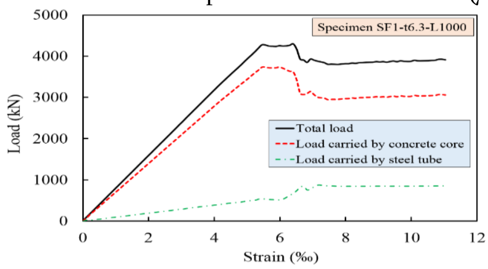

(d) Load distribution of specimen SF1-t6.3-L1000 (μ=0.3)

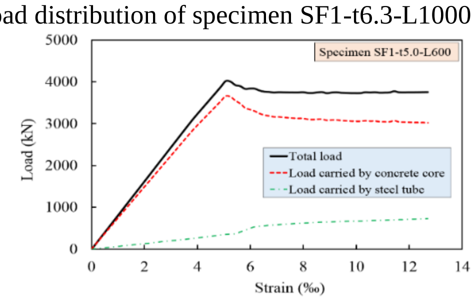

(e) Load distribution of specimen SF1-t5.0-L600 (μ=0.3)

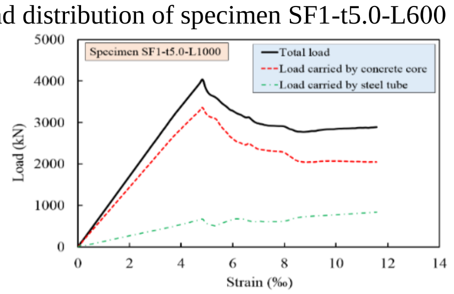

(f) Load distribution of specimen SF1-t5.0-L1000 (μ=0.4)

Fig. 13 Load distribution of selected specimens obtained from FEM results

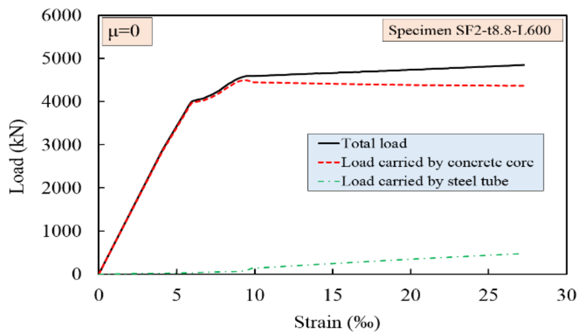

μ = 0.0

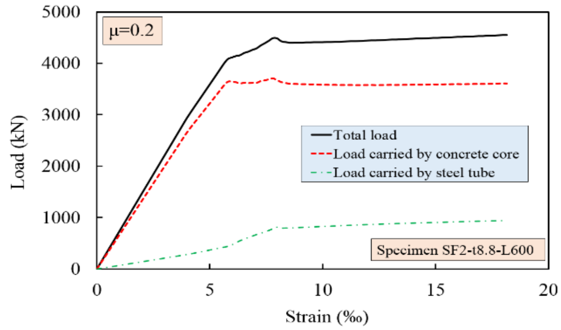

μ = 0.2

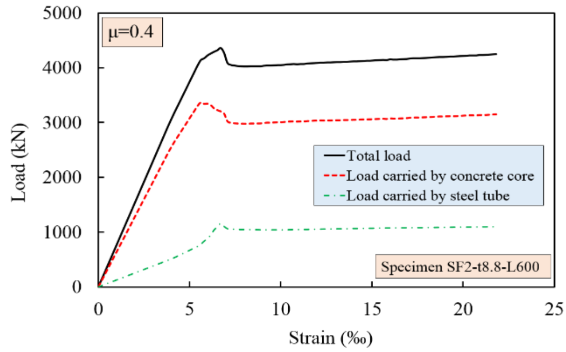

μ = 0.4

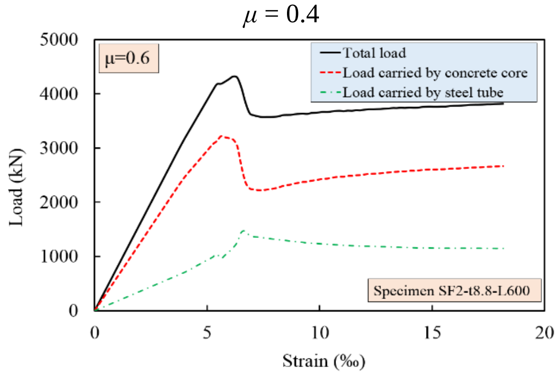

μ = 0.6

Fig. 14 Distribution of load in the midsection of specimen SF2-t8.8-L600 for four friction coefficients μ = 0.0, 0.2, 0.4, 0.6. (Results obtained from FEM)

normalized in relation to the sum of individual resistance of the concrete section and the steel section (A_sf_y+A_cf_c). It can be clearly seen that the ultimate load drastically decreases when the friction coefficient changes from 0 to 0.3, but it tends to slightly decreases when the friction coefficient changes from 0.3 to 0.6.

As also insisted above, the friction coefficient greatly

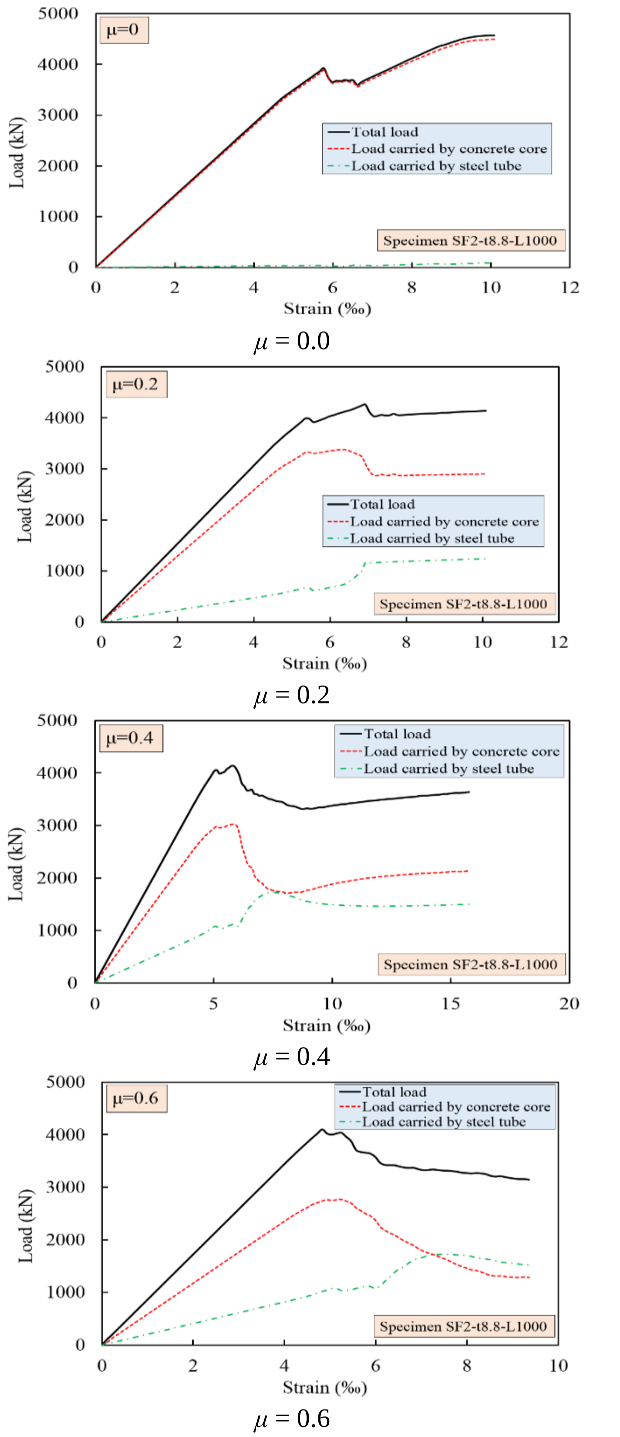

Fig. 15 Distribution of load in the midsection of specimen SF2-t8.8-L1000 for four friction coefficients μ = 0.0, 0.2, 0.4, 0.6 (Results obtained from FEM)

affects not only the ultimate load but also the L-S curve. This is due to the load distribution on the concrete core and the steel tube. For instance, with increasing the friction coefficient, the vertical stress in steel tube increases, while the hoop stress in steel tube decreases. Accordingly, the decrease in the hoop stress of steel tube leads to the decrease in the ultimate load. When the friction coefficient for each tested column was determined using the prediction by the FEM as described above, the load contribution of the concrete core and the steel tube to the total load was also illustrated in Fig. 13 for some selected columns. These figures show how the axial load obtained from FEM in the midsection of the columns is distributed between the concrete core and the steel tube. Furthermore, the effect of the change in the friction coefficients μ = 0, 0.2, 0.4, 0.6 on the load contribution of the concrete core and the steel tube to the total load was performed in Figs. 14-15 for the column SF2-t8.8-L600 and SF2-t8.8-L1000, respectively. It can be seen that the contribution of the concrete core and the steel tube to the total load significantly depends on the friction coefficient. For instance, at the ultimate load, the steel tube contributes approximately 30% to the total load with μ = 0.6, while this contribution is about 10-15% of the total load with μ = 0.3. This finding can be supported by the previous study of Johansson (2002).

Table 2 Comparison of the ultimate loads between FEM and tests

Series	Specimens	$N_{u,test}$ (kN)	$N_{u,FEM}$ (kN)	Friction coefficient μ	$N_{u,FEM}/N_{u,test}$
	SF0-t8.8-L600	4200.84	4220	0.6	1.005
	SF1-t8.8-L600	4288.54	4600	0.6	1.073
	SF2-t8.8-L600	4354.06	4320	0.6	0.992
1	SF0-t8.8-L1000	3919.86	4020	0.5	1.026
	SF1-t8.8-L1000	4178.66	4470	0.5	1.070
	SF2-t8.8-L1000	4099.79	4080	0.5	0.995
	SF0-t6.3-L600	3692.81	4200	0.6	1.137
	SF1-t6.3-L600	3807.97	4380	0.6	1.150
	SF2-t6.3-L600	4033.01	4050	0.6	1.004
2	SF0-t6.3-L1000	3861.14	4110	0.6	1.064
	SF1-t6.3-L1000	3535.31	4280	0.3	1.211
	SF2-t6.3-L1000	3584.70	4020	0.5	1.121
	SF0-t5.0-L600	3645.94	4000	0.3	1.097
	SF1-t5.0-L600	3997.48	4020	0.3	1.006
3	SF2-t5.0-L600	4224.02	3990	0.3	0.945
	SF0-t5.0-L1000	3383.35	3860	0.3	1.141
	SF1-t5.0-L1000	3724.06	4030	0.4	1.082
	SF2-t5.0-L1000	3995.71	3910	0.3	0.979
	Mean				**1.061**
	COV				**0.068**

Fig. 16 displays the deformation of the modelled column SF2-t8.8-L600 (μ =0.6) with the steps before and after the peak load (scale 1:20). The dominant failure mode in FEM is global outward bulge in the middle of the columns. Additionally, the deformation and the Von-Mises stress of only steel tube of the modelled column SF2-t8.8-L600 (μ =0.6) were also demonstrated in Fig. 17 (scale 1:20). The deformation observed in the FEM is not comparable with those obtained from the test results. This is obviously due to the fact that the crack localization cannot be capture with one fourth symmetry of the column in the FEM. Therefore, the FEM was impossible to model the shear failure as observed in the tests.

From the above comparison, it can be concluded that generally good agreement was obtained between FEM

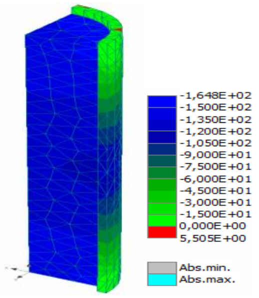

(a) Before the peak load (step 15)

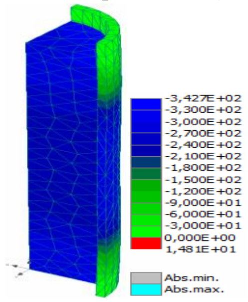

(b) At the peak load (step 34)

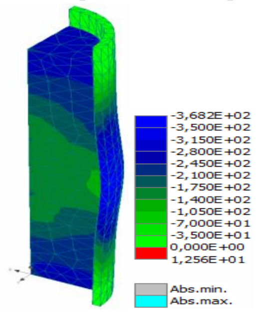

(c) After the peak load (step 50)

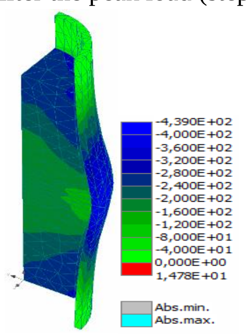

(d) After the peak load (step 100)

Fig. 16 The deformation and the stress in Z direction at different steps of loading

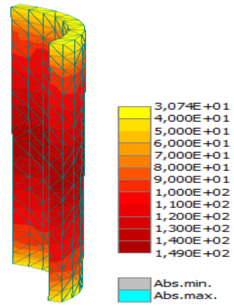

(a) Before the peak load (step 15)

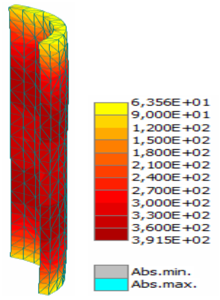

(b) At the peak load (step 34)

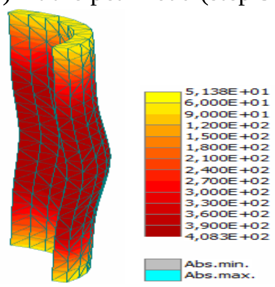

(c) After the peak load (step 50)

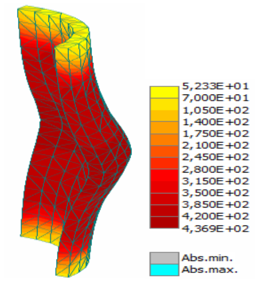

(d) After the peak load (step 100)

Fig. 17 The deformation and the Von-Mises stress of the steel tube at different steps of loading

results and experimental results. As a consequence, the established FEM can be reliably adopted to predict the behavior of CSTCC columns employing UHPC or UHPFRC and to conduct further analysis.

4. Analytical assessment

4.1 Existing analytical models

It is found that up to date, there have been a large number of analytical models to predict the confined compressive strength of concrete (f_{cc}) under lateral confinement provided by steel tube, steel reinforcement, metal strips or other types of confining methods such as using fiber reinforced polyme (FRP), carbon fiber reinforced polyme (CFRP) and aramid fiber reinforced polyme (AFRP). The majority of the existing confined models were developed by deriving from the theoretical models proposed Richart *et al.* (1928) and Mander *et al.* (1988), in which the confined compressive strength (f_{cc}) was a function of the unconfined compressive strength (f_c) and the lateral confining pressure (f_l). The general approach of the existing confined models is the assumption of constant confinement, where the external jacket produces a constant lateral confining pressure on the concrete core. However,

Table 3 Details of the specific models for circular CFST columns

Authors	Expressions	Explanations
Susantha *et al.* (2001)	$v'_c = \frac{0.881}{10^6}\cdot\left(\frac{D}{t}\right)^3 - \frac{2.58}{10^4}\cdot\left(\frac{D}{t}\right)^2 + \frac{1.953}{10^2}\left(\frac{D}{t}\right)+0.4011$ $v_c = 0.2312+0.3528\cdot v'_c - 0.1524\cdot\left(\frac{f_c}{f_y}\right)+4.843\cdot v'_c\left(\frac{f_c}{f_y}\right)-9.169\cdot\left(\frac{f_c}{f_y}\right)^2$ $\beta = v_c - v_s$ and $f_{rp}=\beta\cdot\frac{2\cdot t}{D-2\cdot t}\cdot f_y$ $f_{cc}=f_c+4\cdot f_{rp}$ and $N_u = A_c\cdot f_{cc}+A_s\cdot fy$	v_c and v_s : Poisson ratio of a steel tube filled with concrete and a steel in yield condition f_{rp} : Lateral pressure at the peak load f_{cc} : Confined compressive strength of the concrete N_u : Axial capacity of CFST column
Hatzigeorgiou (2008)	$\sigma_h = f_y\cdot\exp\left[\ln\left(\frac{D}{t}\right)+\ln(f_y)-11\right]$ $f_{rp}=\frac{2\cdot t}{D-2\cdot t}\cdot\sigma_h$ and $f_{cc}=f_c+4.3\cdot f_{rp}$ $f_{yc}=0.5\cdot\left(\sigma_h-\sqrt{4\cdot f_y^2-3\cdot\sigma_h^2}\right)$, $N_u = A_c\cdot f_{cc}+A_s\cdot f_{yc}$	σ_h : Hoop stress of the steel f_{rp} : Mean confining stress f_{yc} : Compressive yield stress of steel tube
Johansson (2002)	$v_a=0.3, v_c=0.2, \varepsilon_v=0.002$ $\varepsilon_{ahr}=\frac{\varepsilon_v(v_a-v_c)}{\left[1+\frac{2\cdot t\cdot E_a}{(D-2\cdot t)\cdot E_c}\right]}$ and $\varepsilon_{ah}=-v_a\cdot\varepsilon_v+\varepsilon_{ahr}$ $\sigma_{ah}=\frac{E_a}{1-v_a^2}\cdot(\varepsilon_{ah}+v_a\cdot\varepsilon_{al});\sigma_{al}=\frac{E_a}{1-v_a^2}\cdot(\varepsilon_v+v_a\cdot\varepsilon_{ah})$ $\sigma_{lat}=\sigma_{ah}\cdot\frac{2\cdot t}{D-2\cdot t}$ and $k=1.25\cdot\left(1+0.062\cdot\frac{\sigma_{lat}}{f_{ct}}\right)\cdot f_c^{-0.21}$ $f_{cc}=f_c\cdot\left(\frac{\sigma_{lat}}{f_{ct}}+1\right)^k$ and $N_u=A_c\cdot f_{cc}+A_s\cdot\sigma_{al}$	v_a, v_c, ε_v : Initial considered values ε_{ahr} : Restrained steel strain ε_{ah} : Final lateral strain of steel σ_{ah} : Steel's lateral stress σ_{al} : Steel's longitudinal stress σ_{lat} : Compressive confining pressure k : Parameter that reflects the effectiveness of confinement f_{ct} : Tensile strength of concrete
Sakino *et al.* (2004)	$\sigma_{ccB}=\gamma_u\cdot f_c+4.1\cdot\sigma_r$, $\gamma_u=1.67\cdot D_c^{-0.112}$ $\sigma_r=\frac{-2\cdot t}{D-2\cdot t}\cdot\sigma_{s\theta}$, $\sigma_{s\theta}=\alpha_u\cdot\sigma_{sy}$ and $\sigma_{sz}=\beta_{uc}\cdot\sigma_{sy}$, $\alpha_u=-0.19;\beta_{uc}=0.89$ $N_u=A_c\cdot\sigma_{ccB}+A_s\cdot\sigma_{sz}$	σ_{ccB} : Strength of confined concrete γ_u : Strength reduction factor for concrete and σ_r : Lateral pressure $\sigma_{s\theta}$: Hoop stress of steel tube in yield condition and σ_{sy} : Tensile yield stress of steel σ_{sz} : Axial yield stress of steel tube
Liang and Fragomeni (2009)	$f_{cc}=\gamma_c\cdot f_c+k_1\cdot f_{rp}$ $f_{rp}=\begin{cases}0.7\cdot(v_e-v_s)\cdot\frac{2\cdot t}{D-2\cdot t}\cdot f_{sy}\left(\frac{D}{t}\le 47\right)\\ \left(0.006241-0.0000357\cdot\frac{D}{t}\right)\cdot f_{sy}\left(47<\frac{D}{t}\le 150\right)\end{cases}$ $v_e=0.2312+0.3528\cdot v'_e-0.1524\cdot\left(\frac{f_c}{f_{sy}}\right)+4.843\cdot v'_c\left(\frac{f_c}{f_{sy}}\right)-9.169\cdot\left(\frac{f_c}{f_{sy}}\right)^2$ $v'_e=\frac{0.881}{10^6}\cdot\left(\frac{D}{t}\right)^3-\frac{2.58}{10^4}\cdot\left(\frac{D}{t}\right)^2+\frac{1.953}{10^2}\left(\frac{D}{t}\right)+0.4011$ $\gamma_c=1.85\cdot D_c^{-0.135}(0.85\le\gamma_c\le 1)$, $\gamma_s=1.458\cdot\left(\frac{D}{t}\right)^{-0.1}(0.9\le\gamma_s\le 1.1)$ $N_u=(\gamma_c\cdot f_c+4.1\cdot f_{rp})\cdot A_c+\gamma_s\cdot f_{sy}\cdot A_s$	f_{cc} : Strength of confined concrete f_{rp} : Lateral pressure γ_c : Strength reduction factor for concrete γ_s : Strength factor for the steel tube f_{sy} : Tensile yield strength of steel v'_e : Empirical factor v_e : Poisson ratio of a steel tube filled with concrete

the substantial discrepancy among the existing confined models is the lateral confining pressure that the authors assume to calculate the increased strength of the concrete core. The effective confining pressure at the ultimate state of the confined columns is quantified in most of the confined models directly through the empirical formula or

Table 4 Details of the conventional models for confined concrete

Authors	Expressions
Richart *et al.* (1928)	$f_{cc} = f_c[1+4.1 f_l]$
Mander *et al.* (1988)	$f_{cc} = f_c\left[2.254\sqrt{1+7.94\frac{f_l}{f_c}} - 2\frac{f_l}{f_c} - 1.254\right]$
Saatcioglu and Razvi (1992)	$f_{cc} = f_c + 6.7 f_l^{0.83}$
Cusson and Paultre (1995)	$f_{cc} = f_c\left[1+2.1\left(\frac{f_l}{f_c}\right)^{0.7}\right]$
Ahmad and Shah (1982)	$f_{cc} = f_c\left[1+4.2556\frac{f_l}{f_c}\right]$ $\left(\frac{f_l}{f_c} < 0.68\right)$ $f_{cc} = f_c\left[1.7757+3.1171\frac{f_l}{f_c}\right]$ $\left(\frac{f_l}{f_c} \geq 0.68\right)$
Attard and Setunge (1996)	$f_{cc} = f_c\left[1+\frac{f_l}{f_t}\right]^k$, $k = 1.25\left[1+0.062\frac{f_l}{f_c}\right]f_c^{-0.21}$ f_t is the tensile strength of the concrete core
Bing *et al.* (2001)	$f_{cc} = f_c\left[1.413\sqrt{1+11.4\frac{f_l}{f_c}} - 2\frac{f_l}{f_c} - 0.413\right]$
Setunge *et al.* (1993)	$f_{cc} = f_c\left[1+13.07\frac{f_l}{f_t}\right]^{0.63}$ $(20MPa \leq f_c \leq 50MPa)$ $f_{cc} = f_c\left[1+18.67\frac{f_l}{f_t}\right]^{0.45}$ $(90MPa \leq f_c \leq 132MPa)$
Legeron and Paultre (2003)	$f_{cc} = f_c\left[1+2.4\left(\frac{f_l}{f_c}\right)^{0.7}\right]$
Girgin *et al.* (2007)	$f_{cc} = f_c\left[1+4.08\left(\frac{f_l}{f_c}\right)^{0.83}\right]$
Newman and Newman (1971)	$f_{cc} = f_c\left[1+3.7\left(\frac{f_l}{f_c}\right)^{0.86}\right]$
Xiao *et al.* (2010)	$f_{cc} = f_c\left[1+3.24\left(\frac{f_l}{f_c}\right)^{0.8}\right]$
EC2 (2004)	$f_{cc} = f_c\left[1+5\frac{f_l}{f_c}\right]$ $(f_l < 0.05 f_c)$ $f_{cc} = f_c\left[1.125+2.5\frac{f_l}{f_c}\right]$ $(f_l > 0.05 f_c)$

applying the yield of external jacket material (e.g., Mander *et al.* 1988, Saatcioglu and Razvi 1992). In constrast, in some other models, the variation of hoop stress in the elastic stage is taken into account by using the iterative procedure at each level of axial strain of the concrete core and the compatibility between the concrete core and the external jacket material is considered (e.g., Ahmad and Shah 1982, Cusson and Paultre 1995).

There are some confined models directly developed for the concrete confined by the steel tube. Liang and Fragomeni (2010), and Susantha *et al.* (2007) used the Poisson's ratio of the steel tube and the concrete core at the ultimate state in the calculation of the lateral confining pressure. Hatzigeogiou (2008) and Sakino *et al.* (2004) empirically suggested formulae for prediction of the peak confined strength of the concrete core in CFST columns with considering the hoop and longitudinal stress of the steel tube at the ultimate condition. In a different manner, Johansson (2002) proposed a volumetric strain model deriving from the dilatation of the concrete core and the steel tube in each step of loading and the strain compatibility of two these materials, thereby establishing a full stress-strain model for confined concrete in circular CFST columns with some modifications to the ealier model of Sargin (1971).

It is revealed from the review of the available confinement models that the majority of these models are applicable for NSC or HSC, while their suitability for UHPC and UHPFRC is still questionable. Therefore, the evaluation of existing confined models is needed for circular STCC columns with the employment of UHPC and UHPFRC. This work shall provide a meaningful supplement to the previous studies by De Oliveira *et al.* (2010) and Liu *et al.* (2018) as mentioned in the introduction section. In this study, the collected confined models were divided into two group: (1) five specific models developed for only confined concrete in CFST columns include Susantha *et al.* (2001), Johansson (2002), Hatzigeorgiou (2008), Liang and Fragomeni (2009), Sakino *et al.* (2004), (2) thirteen conventional models developed for confined concrete include Mander *et al.* (1988), Richart *et al.* (1928), Saatcioglu and Razvi (1992), Cusson and Paultre (1995), Newman and Newman (1971), Attard and Setunge (1996), Setunge *et al.* (1993), Legeron and Paultre (2003), Girgin *et al.* (2007), Amad and Shah (1982), Xiao *et al.* (2010), Bing *et al.* (2001), Eurocode 2-EC2 (2004). The formulae for prediction of confined peak strength (f_{cc}) of the selected models in group 1 and group 2 are given in Table 3 and Table 4, respectively. It is worth noting that there were some limitations on the concrete strength in the previous confined models. Ealier models by Richart *et al.* (1928), Mander *et al.* (1988), Saatcioglu and Razvi (1992), Newman and Newman (1971) were proposed for NSC with cylinder compressive strenth up to 50 MPa, while the remaining conventional models and the five specific models for CFST columns allowed the use of HSC up to 90 MPa. Likewise, as an international code, EC2 (2004) covered the concrete strength up to 90 MPa. In particular, some models can be adopted for UHSC higher than 90 MPa, for instance, the models by Girgin *et al.* (2007) and Setunge *et al.* (1993) extended the concrete strength up to 132 MPa, while the model by Legeron and Pautre (2003) was applicable to concrete strength of 120 MPa.

Based on the critical review on the selected models as mentioned above, an attempt were made in this study to evaluate the suitability of these models with respect to the prediction of the peak confined strength (f_{cc}) for eighteen CSTCC short and intermediate columns using UHPC and UHPFRC having cylinder compressive strength ranging from 178.9 MPa to 198 MPa. It is regconized that the prediction obtained from selected models might be

Table 5 Comparison of the peak confined strength between the conventional models and the test results

Specimens	$f_{cc,test}$ (MPa)	$f_{cc,pre}$ (MPa)							
		Mander *et al.* (1988)	Bing *et al.* (2001)	Attard and Setunge (1996)	Cusson and Paultre (1995)	Setunge *et al.* (1992)	Richart *et al.* (1928)	Legeron and Paultre (2003)	Girgin *et al.* (2007)
SF0-t8.8-L600	294.50	299.40	272.71	297.23	263.66	306.57	270.45	276.58	308.89
SF1-t8.8-L600	300.65	316.97	290.43	315.05	281.44	324.81	285.78	294.67	326.17
SF2-t8.8-L600	305.24	309.96	283.30	307.91	274.24	317.52	279.65	287.36	319.29
SF0-t6.3-L600	240.70	285.41	267.70	286.25	262.86	293.20	257.83	273.03	291.94
SF1-t6.3-L600	248.20	282.65	264.93	283.41	260.02	290.35	255.26	270.15	289.14
SF2-t6.3-L600	262.87	274.80	257.03	275.31	251.89	282.24	247.98	261.91	281.20
SF0-t5.0-L600	229.04	273.41	256.64	274.28	252.14	280.89	247.07	261.82	279.64
SF1-t5.0-L600	251.13	279.17	262.41	280.20	258.06	286.82	252.43	267.83	285.48
SF2-t5.0-L600	265.36	276.58	259.76	277.51	255.29	284.15	249.99	265.05	282.86
SF0-t5.0-L1000	212.55	245.86	230.78	246.64	226.73	252.58	222.17	235.44	251.46
SF1-t5.0-L1000	233.95	250.63	235.58	251.56	231.67	257.50	226.62	240.45	256.30
SF2-t5.0-L1000	251.02	247.69	232.62	248.52	228.62	254.47	223.88	237.36	253.31
SF0-t6.3-L1000	251.67	257.09	241.14	257.85	236.78	264.10	232.24	245.94	262.97
SF1-t6.3-L1000	230.43	254.29	238.35	254.96	233.93	261.21	229.65	243.04	260.12
SF2-t6.3-L1000	233.65	247.46	231.46	247.92	226.83	254.16	223.31	235.85	253.22
SF0-t8.8-L1000	274.80	269.19	245.19	267.24	237.06	275.64	243.16	248.67	277.72
SF1-t8.8-L1000	292.95	285.64	261.72	283.90	253.61	292.70	257.52	265.54	293.93
SF2-t8.8-L1000	287.42	278.45	254.49	276.60	246.36	285.24	251.21	258.15	286.82
Mean value of $f_{cc,pre}/f_{cc,test}$		**1.063**	**0.989**	**1.063**	**0.967**	**1.091**	**0.960**	**1.007**	**1.089**
Deviation of $f_{cc,pre}/f_{cc,test}$		**0.067**	**0.076**	**0.070**	**0.081**	**0.068**	**0.068**	**0.078**	**0.065**

Table 6 Comparison of the peak confined strength between the conventional models and the test results (continued)

Specimens	$f_{cc,test}$ (MPa)	$f_{cc,pre}$ (MPa)					
		Newman and Newman (1971)	Ahmad and Shah (1982)	Saatcioglu and Razvi (1992)	Xiao *et al.* (2010)	EC2(2004)	FEM in this study
SF0-t8.8-L600	294.50	289.13	274.14	265.47	287.58	195.23	295.84
SF1-t8.8-L600	300.65	305.85	289.46	280.81	304.91	212.73	322.48
SF2-t8.8-L600	305.24	299.17	283.34	274.67	297.96	205.49	302.85
SF0-t6.3-L600	240.70	276.09	260.34	258.68	277.43	215.83	262.02
SF1-t6.3-L600	248.20	273.37	257.77	256.11	274.64	212.99	291.36
SF2-t6.3-L600	262.87	265.63	250.49	248.83	266.68	204.75	265.94
SF0-t5.0-L600	229.04	264.55	249.45	248.46	265.89	207.59	263.85
SF1-t5.0-L600	251.13	270.24	254.81	253.82	271.72	213.53	275.16
SF2-t5.0-L600	265.36	267.66	252.38	251.39	269.06	210.60	254.43
SF0-t5.0-L1000	212.55	237.89	224.32	223.43	239.10	186.68	258.20
SF1-t5.0-L1000	233.95	242.61	228.76	227.87	243.94	191.70	268.88
SF2-t5.0-L1000	251.02	239.70	226.02	225.13	240.95	188.60	252.54
SF0-t6.3-L1000	251.67	248.70	234.51	233.01	249.90	194.41	260.72
SF1-t6.3-L1000	230.43	245.94	231.90	230.41	247.08	191.61	262.02
SF2-t6.3-L1000	233.65	239.20	225.57	224.08	240.15	184.38	260.07
SF0-t8.8-L1000	274.80	259.96	246.48	238.69	258.57	175.53	270.61
SF1-t8.8-L1000	292.95	275.62	260.84	253.05	274.77	191.70	282.52
SF2-t8.8-L1000	287.42	268.75	254.53	246.74	267.67	184.59	274.11
Mean value of $f_{cc,pre}/f_{cc,test}$		**1.027**	**0.970**	**0.957**	**1.029**	**0.773**	**1.062**
Deviation of $f_{cc,pre}/f_{cc,test}$		**0.068**	**0.067**	**0.075**	**0.071**	**0.117**	**0.077**

inadequate for the columns using higher concrete strength with an overestimation, especially for UHPC or UHPFRC. Moreover, the previous models were built up for only short columns and their approriateness for intermediate columns should be further clarified. The lateral confining pressure in most of the conventional confined models was established for the confined concrete with internal tranverse reinforcement, while the specific confined models was calibrated for CFST column under loading on entire section. In both CFST columns and STCC column with bonding between two materials due to the natural roughness surfaces, the steel tube carries the axial load. In STCC columns, although only the concrete core is loaded, the axial load is transmitted to the steel tube through the interfacial bond beween two materials, thus inducing the longitudinal stress in the steel tube. The hoop stress in the steel tube provides the lateral confining pressure on the concrete core, thereby leading to an increased strength for the concrete core. It should be mentioned that, only in the case of STCC column without bonding between the steel tube and the concrete core, the steel tube does not carry the longitudinal load and only the hoop stress is induced to confine the concrete core. In this case, the confinement effect becomes to be maximal. The basic difference between the models of CFST columns and STCC columns is the proportion of the longitudinal and hoop stresses of the steel tube. In general, the mechanism of two columns types is similar. From this finding, the specific confined models for CFST columns can be adopted for STCC columns. This work was also investigated by De Oliveira *et al.* (2010).

To avoid the large overestimation of the peak confined strength for the conventional models as compared to the test results, the lateral confining pressure f_l of all models in Table 4 was calculated using the study of Liu *et al.* (2016)

$$f_l = \frac{1.08 t f_y}{D - 2t} \tag{12}$$

The correction factor $\lambda_{Oliveira}$ for the columns having $L/D \geq 3$ (Eq. (14)), which was suggested by De Oliveira *et al.* (2010), was adopted in the formula for prediction of f_{cc}

$$f_{cc,pre} = f_{cc,pre1} \cdot \lambda_{Oliveira} \tag{13}$$

$$\lambda_{Oliveira} = -0.18 \ln\left(\frac{L}{D}\right) + 1.2 \tag{14}$$

in which $f_{cc,pre1}$ is the peak confined strength predicted using the original formulae of the selected models in Table 4, $f_{cc,pre}$ is the peak confined strength after using the correction factor $\lambda_{Oliveira}$.

4.2 Comparison of model predictions with test results

The calculated peak confined strength ($f_{cc,pre}$) obtained from previous models and corresponding experimental results (f_{cc}) were given in Tables 5-7. To clarify the variability between the predictions and the measured

Table 7 Comparison of the peak confined strength between the specific models and the test results

Specimens	$f_{cc,test}$ (MPa)	$f_{cc,pre}$ (MPa)				
		Susantha *et al.* (2001)	Johansson (2002)	Hatzigeorgiou (2008)	Liang and Fragomeni (2009)	Sakino *et al.* (2004)
SF0-t8.8-L600	294.50	291.50	309.60	296.84	347.86	299.84
SF1-t8.8-L600	300.65	312.38	326.94	312.09	328.20	314.52
SF2-t8.8-L600	305.24	303.77	320.02	306.05	338.13	308.74
SF0-t6.3-L600	240.70	273.98	288.90	275.26	275.06	270.04
SF1-t6.3-L600	248.20	270.64	286.08	272.68	276.52	267.56
SF2-t6.3-L600	262.87	261.11	278.10	265.41	281.20	260.58
SF0-t5.0-L600	229.04	248.49	257.78	268.45	249.15	256.15
SF1-t5.0-L600	251.13	254.47	263.53	273.84	258.62	261.31
SF2-t5.0-L600	265.36	251.65	260.89	271.46	253.64	259.03
SF0-t5.0-L1000	212.55	223.45	231.81	241.40	224.05	230.34
SF1-t5.0-L1000	233.95	228.46	236.59	245.84	232.18	234.60
SF2-t5.0-L1000	251.02	225.36	233.64	243.10	227.15	231.97
SF0-t6.3-L1000	251.67	246.80	260.23	247.94	247.76	243.24
SF1-t6.3-L1000	230.43	243.48	257.37	245.32	248.77	240.71
SF2-t6.3-L1000	233.65	235.13	250.43	239.00	253.23	234.66
SF0-t8.8-L1000	274.80	262.09	278.36	266.88	312.76	269.59
SF1-t8.8-L1000	292.95	281.49	294.62	281.24	295.75	283.43
SF2-t8.8-L1000	287.42	272.88	287.48	274.93	303.75	277.35
Mean value of $f_{cc,pre}/f_{cc,test}$		**1.007**	**1.057**	**1.039**	**1.060**	**1.019**
Deviation of $f_{cc,pre}/f_{cc,test}$		**0.060**	**0.062**	**0.064**	**0.066**	**0.054**

results, the mean value and the deviation of the ratios $f_{cc,pre}/f_{cc}$ were computed and also shown in Tables 5-7. Figs. 18-19 graphically shows the relation between the ratios $f_{cc,pre}/f_{cc}$ and the confinement index ξ. As can be observed in these tables, except for EC2 (2004), all selected models exhibited a good prediction on the peak confined strength with small mean values of the ratios $f_{cc,pre}/f_{cc}$ ranging from 0.7% to 9.1% and small deviations of the ratios $f_{cc,pre}/f_{cc}$ varying between 5.4% and 8.1%. Among selected models, on average, the peak confined strength was highly underestimated by 27% in EC2 (2004) and overestimated by 9.1% in the model of Setunge *et al.* (1992). In terms of the conventional models, the predictions by the models of Bing *et al.* (2001), Cusson and Paultre (1995), Richart *et al.* (1928), Girgin *et al.* (2007), Ahmad and Shah (1982), Saatcioglu and Razvi (1992) were conservative, whereas the remaining models gave slight overestimations. With regard to the specific models, the predictions by all models were unconservative. Deriving from this comparison, except for EC2 (2004), all selected models can be applicable to accurately predict the peak confined strength of CSTCC columns using UHPC and UHPFRC. Meanwhile, the FEM gave a slight overestimation with the mean value of 6.2% and the deviation of 7.7%, thus indicating that the established FEM can be suitably adopted. It is worth noting that the model by Bing *et al.* (2001) performed the best prediction as compared to other models with the mean value of 1.1% and the deviation of 7.6%. Furthermore, the model of Bing *et al.* (2001) provided an conservative

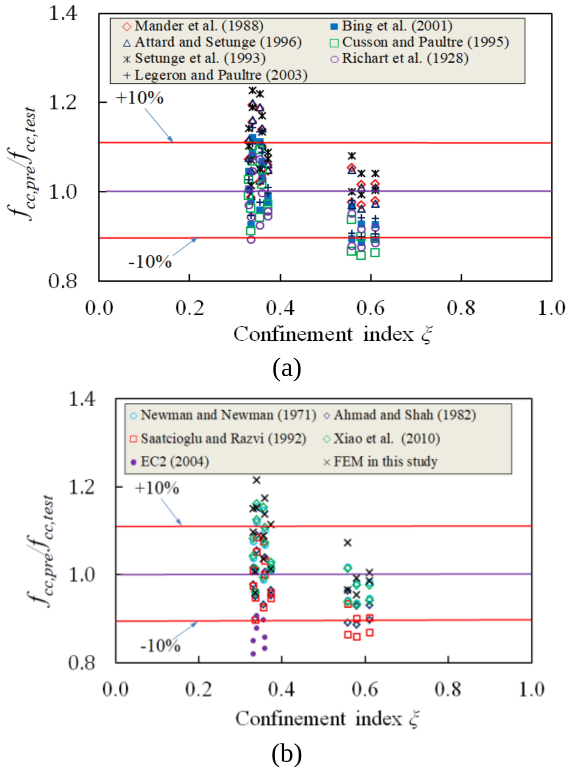

Fig. 18 The relation between $f_{cc,pre}/f_{cc,test}$ and the confinement index ξ for conventional models

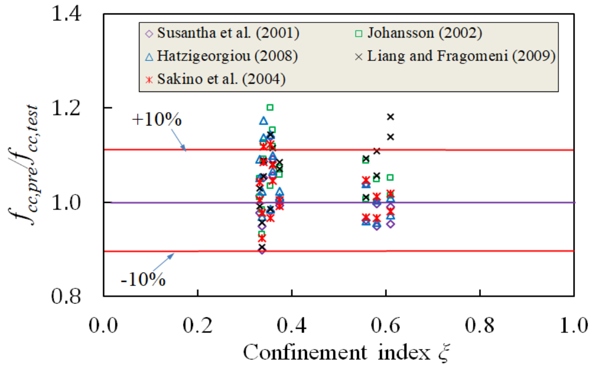

Fig. 19 The relation between $f_{cc,pre}/f_{cc,test}$ and the confinement index ξ for specific models

approximation of the peak confined strength, being on the safe side. As a consequence, the model of Bing *et al.* (2001) can be chosen as the best predictor.

It can be briefly concluded that with the assisstance of Eqs. (12)-(14), the predictions by all selected models except for EC2 (2004) gave a very good agreement with the test results. From this finding, all these models, particularly the model of Bing *et al.* (2001) can be reasonably used by engineers in practice to predict the peak confined strength of CSTCC stub and intermediate columns with UHPC and UHPFRC infilled.

5. Conclusions

This paper developed a FEM with the assistance of

ATENA-3D software to investigate the axially compressive behavior of CSTCC columns using UHPC and UHPFRC. Besides, eighteen confined concrete models were modified and used to predict the peak confined strength to assess their applicability for UHPC and UHPFRC. On the basis of the reported findings and within the investigated configuration, the following conclusions can be drawn:

• The results of established FEM in ATENA-3D with the choice of the best suitable friction coefficient were in a good agreement with the test results. Therefore, the FEM can be reliably used to predict the behavior of CSTCC stub and intermediate columns using UHPC and UHPFRC under axial loading.

• The axial compressive behavior and the load distribution between the concrete core and the steel tube are significantly affected by the change of friction coefficient. The result of parametric study on six values of friction coefficients indicated the suitable friction coefficient for each tested columns.

• The increase in the friction coefficient results in a greater contribution from the steel tube, i.e., the load portion in steel tube and the initial stiffness of the columns are increased.

• The ultimate load of the columns decreases with decreasing the friction coefficient. In the FEM, the ultimate load drastically decreases when the friction coefficient varies from 0 to 0.3, but it tends to slightly decreases when the friction coefficient changes from 0.3 to 0.6.

• The magnitude of the loss of load capacity right after the ultimate load in the FEM increases with increasing the friction coefficient.

• The appropriate friction coefficient between the steel tube and the concrete core was defined as 0.3 to 0.6.

• The equation for predicting the lateral confining stress (Eq. (12)) and the equation for considering the column slenderness (Eq. (14)) were proposed and adopted in the selected models (Eq. (13)) to cope with the CSTCC short and intermediate columns.

• Except for EC2 (2004), all selected models including the conventional models and specific models with the modification (Eq. (13)) can be reasonably used to predict the confined peak strength of CSTCC columns infilled with UHPC and UHPFRC.

• Among the selected models, the model of Bing *et al.* (2001) was the best predictor.

Acknowledgments

The funding for this study was provided by Kassel Univrsity, Ton Duc Thang University and Duy Tan University. The authors would like to greatly appreciate their financial support. This work was also supported by the National Research Foundation of Korea (NRF) grant funded by the Korea government (MSIT) (No. 2018R1C1B5086385).

References

Aboutaha, R.S. and Machado, R. (1998), "Seismic resistance of steel confined reinforced concrete (SCRC) columns", *Struct. Des. Tall Build.*, **7**(3), 251-260.

Ahmad, S.H. and Shah, S.P. (1982), "Complete triaxial stress-strain curves for concrete", *J. Struct. Eng.*, **108**(4), 728-742.

Aly, T., Eichalakami, M. and Thayalan, P. (2010), "Incremental collapse threshold for push-out resistance of circular concrete filled steel tubular columns", *J. Constr. Steel Res.*, **66**(1), 11-18.

An, L.H. and Fehling, E. (2016b), "Finite element analysis of circular steel tube confined UHPC stub columns", *Proceedings of the 1st International Conference on UHPC Materials and Structures*, Changsha, China, October.

An, L.H. and Fehling, E. (2017a), "A review and analysis of UHPC filled steel tube columns", *Struct. Eng. Mech.*, **61**(2), 417-430.

An, L.H. and Fehling, E. (2017b), "Analysis of circular steel tube confined UHPC stub columns", *Steel Compos. Struct.*, **23**(6), 669-682.

An, L.H. and Fehling, E. (2017c), "Assessment of axial stress-strain model for UHPC confined by circular steel tube stub columns", *Struct. Eng. Mech.*, **3**(3), 371-384.

An, L.H. and Fehling, E. (2017d), "Influence of steel fiber content and type on the uniaxial tensile and compressive behavior of UHPC", *Constr. Build. Mater.*, **153**, 790-806.

An, L.H. and Fehling, E. (2017e), "Numerical analysis of steel tube confined UHPC stubs columns", *Comput. Concrete*, **19**(3), 263-273.

An, L.H. and Fehling, E. (2017f), "Numerical study of circular steel tube confined concrete (STCC) stub columns with various concrete strengths", *J. Constr. Steel Res.*, **136**, 238-255.

An, L.H. and Fehling, E. (2017g), "Effect of steel fiber on the behavior of circular steel tube confined UHPC columns under axial loading", *Proceedings of the 4th International Conference on Strain-Hardening Cement-Based Composites*, Dresden, Germany, September.

An, L.H. and Fehling, E. (2017h), "Experimental study on the compressive behavior of circular steel tube confined UHPC columns", *Proceedings of the 16th International Symposium on Tubular Structures*, Monash, Australia, December.

An, L.H., Fehling, E. and Ismail, M. (2016a), "Numerical modelling of circular concrete filled steel tube stub columns", *Proceedings of the HiperMat 4th International Symposium on Ultra-High Performance Concrete and High Performance Construction Materials*, Kassel, Germany, March.

An, L.H., Fehling, E., Binglin, L., Duc-Kien, T. and Van-Chau, N. (2019a), "Experimental study on structural performance of UHPC and UHPFRC columns confined with steel tube", *Eng. Struct.*, **187**, 457-477.

An, L.H., Fehling, E., Duc-Kien, T. and Van-Chau, N. (2019b), "Evaluation of axial strength in circular STCC columns using UHPC and UHPFRC", *J. Constr. Steel Res.*, **153**, 533-549.

Attard, M.M. and Setunge, S. (1996), "Stress-strain relationship of confined and unconfined concrete", *ACI Mater. J.*, **93**(5), 432-442.

Baltay, P. and Gjelsvik, A. (1990), "Coefficient of friction for steel on concrete at high normal stress", *J. Mater. Civil Eng.*, **2**(1), 46-49.

Bing, L., Park, K. and Tanaka, H. (2001), "Stress-strain behaviour of high strength concrete confined by ultra high and normal strength transverse reinforcements", *ACI Struct. J.*, **98**(3), 395-406.

CEB-FIB (1990), *Structural Concrete-Textbook on Behaviour, Design and Performances (Updated knowledge of CEB/FIP Model Code 1990)*, Volume 1-fib-International Federation for Structural Concrete (fib), Lausanne, Switzerland.

Cervenka, V., Jendele, L. and Cervenka, J. (2013), *ATENA Program Documentation Part 1-Theory*, Cervenka Consulting s.r.o, Na Hrebenkach 55, 150 00 Prague, Czech Republic.

Cusson, D. and Paultre, P. (1995), "Stress-strain model for confined high strength concrete", *J. Struct. Eng.*, **121**(3), 468-477.

De Oliveira, W.L.A., De Nardin, S., De Cresce El Debs, A.L.H. and El Debs, M.K. (2010), "Evaluation of passive confinement in CFT columns", *J. Constr. Steel Res.*, **66**(4), 487-495.

Ding, F.X., Tan, L., Liu, X.M. and Wang, L. (2017), "Behavior of circular thin-walled steel tube confined concrete stub columns", *Steel Compos. Struct.*, **3**(2), 229-238.

Eurocode 2 (EC2 2004), *Design of Concrete Structures-Part 1-1: General Rules and Rules for Building*, EN 1992-1-1:2004, European Standard.

Fam, A., Qie, F.S. and Rizkalla, S. (2004), "Concrete-filled steel tubes subjected to axial compression and lateral cyclic loads", *J. Struct. Eng.*, **130**(4), 631-640.

Fehling, E., Bunje, K. and Leutbecher, T. (2004), "Design relevant properties of hardened ultra high performance concrete", *Proceedings of the International Symposium on Ultra High Performance Concrete*, Kassel, Germany, September.

Fehling, E., Schmidt, M., Walraven, J., Leutbecher, T. and Fröhlich, S. (2014), *Ultra-High Performance Concrete: Fundamental-Design-Example*, Wilhelm Ernst & Sohn, Verlag Für Architektur und Technische Wissenschaften GmbH & Co. KG, Berlin, Germany.

Girgin, Z.C., Arıoglu, N. and Arıoglu, E. (2007), "Evaluation of strength criteria for very-high-strength concretes under triaxial compression", *ACI Struct. J.*, **104**(S27), 277-283.

Graybeal, B.A. (2005), "Characterization of the behavior of ultra-high performance concrete", Ph.D. Dissertation, University of Maryland, U.S.A.

Haghinejad, A. and Nematzadeh, M. (2016), "Three-dimensional finite element analysis of compressive behavior of circular steel tube-confined concrete stub columns by new confinement relationships", *Lat. Am. J. Sol. Struct.*, **13**(5), 916-944.

Han, L.H., Li, W. and Bjorhovde, R. (2014), "Development and advanced applications of concrete-filled steel tubular (CFST) structures: members", *J. Constr. Steel Res.*, **100**, 211-228.

Han, L.H., Liu, W. and Yang, Y.F. (2008), "Behavior of thin walled steel tube confined concrete stub columns subjected to axial local compression", *Thin-Wall. Struct.*, **46**(2), 155-164.

Han, L.H., Yao, G.H., Chen, Z.P. and Yu, Q. (2005), "Experimental behavior of steel tube confined concrete (STCC) columns", *Steel Compos. Struct.*, **5**(6), 459-84.

Hassanein, M.F. and Patel, V.I. (2018), "Roun-ended rectangular concrete-filled steel tubular short columns: FE investigation under axial compression", *J. Constr. Steel Res.*, **140**, 222-236.

Hatzigeorgiou, G.D. (2008), "Numerical model for the behavior and capacity of circular CFT columns, Part I: Theory", *Eng. Struct.*, **30**(6), 1573-1578.

Huang, F., Yu, X. and Chen, B. (2012), "The structural performance of axially loaded CFST columns under various loading conditions", *Steel Compos. Struct.*, **13**(5), 451-471.

Ismail, M., Fehling, E. and An, L.H. (2016), "Comparative analytical Modelling of reinforced UHPCFRC under Pure Torsion", *Proceedings of HiperMat 4th International Symposium on Ultra-High Performance Concrete and High Performance Construction Materials*, Kassel, Germany, March.

Johansson, M. (2002), "Composite action and confinement effects in tubular steel-concrete columns", Ph.D. Dissertation, Chalmers University of Technology, Göteborg, Sweden.

Johansson, M. and Gylltoft, K. (2002), "Mechanical behavior of circular steel-concrete composite stub columns", *J. Struct. Eng.*, **128**(8), 1073-1081.

Kang, S.T. and Kim, J.K. (2011), "The relation between fiber orientation and tensile behavior in an ultra high performance fiber reinforced cementitious composites (UHPFRCC)", *Cement Concrete Res.*, **41**(10), 1001-1014.

Legeron, F. and Paultre, P. (2003), "Uniaxial confinement for normal and high-strength concrete columns", *J. Struct. Eng.*, **129**(2), 241-252.

Liang, Q.Q. and Fragomeni, S. (2009), "Nonlinear analysis of circular concrete-filled steel tubular short columns under axial loading", *J. Constr. Steel Res.*, **65**(12), 2186-2196.

Liew, J.Y.R. and Xiong, D.X. (2010), *Experimental Investigation on Tubular Columns Infilled with Ultra-High Strength Concrete*, Tubular Structures XIII, The University of Hong Kong, Hong Kong.

Liew, J.Y.R. and Xiong, D.X. (2012), "Ultra-high strength concrete filled composite columns for multi-storey building construction", *Adv. Struct. Eng.*, **15**(9), 1487-1503.

Liew, J.Y.R. and Xiong, D.X. (2015), *Design Guide for Concrete Filled Tubular Members with High Strength Materials to Eurocode 4*, Research Publishing, Singapore.

Liew, J.Y.R., Xiong, M.X. and Xiong, D.X. (2016), "Design of concrete filled tubular beam-columns with high strength steel and concrete", *Struct.*, **8**, 215-221.

Liew, J.Y.R., Xiong, M.X. and Xiong, D.X. (2014), "Design of high strength concrete filled tubular columns for tall buildings", *Int. J. High-Rise Build.*, **3**(3), 215-221.

Lim, J.C. and Ozbakaloglu, T. (2015), "Influence of size and slenderness on compressive strain softening of confined and unconfined concrete", *J. Mater. Civil Eng.*, **28**(2), 06015010.

Liu, J., Zhang, S., Zhang, X. and Guo, L. (2009), "Behavior and strength of circular tube confined reinforced-concrete (CTRC) columns", *J. Constr. Steel Res.*, **65**(7), 1447-1458.

Liu, J., Zhou, X. and Gan, D. (2016), "Effect of friction on axially loaded stub circular tubed columns", *Adv. Struct. Eng.*, **19**(3), 546-559.

Liu, J.L., Teng, Y., Zhang, Y., Wang, X. and Chen, Y.F (2018), "Axial stress-strain behavior of high strength concrete confined by circular thin-walled steel tubes", *Constr. Build. Mater.*, **177**, 366-377.

Mander, B.J., Priestley, M.J.N. and Park, R. (1988), "Theoretical stress-strain model for confined concrete", *J. Struct. Eng.*, **114**(8), 1804-1826.

Newman, K. and Newman, J.B. (1971), "Failure theories and design criteria for plain concrete", *Proceedings of the International civil Engineering Materials Conference on Structures, Solid Mechanics, and Engineering Design*, Wiley Interscience, New York, U.S.A.

O'Shea, M.D. and Bridge, R.Q. (1994), "Test of thin-walled concrete-filled steel tubes", *Proceedings of the 12th International Specialty Conference on Cold-Formed Steel Structures*, Missouri, U.S.A.

O'Shea, M.D. and Bridge, R.Q. (2000), "Design of circular thin-walled concrete filled steel tubes", *J. Struct. Eng.*, **126**(11), 1295-1303.

Orito, Y., Sato, Y., Tanaka, N. and Watanabe, K. (1987), "Study on the unbonded steel tube concrete structure", *Proceedings of the Engineering Foundation Conference on Composite Constructions*, Henniker, New Hampshire, U.S.A.

Rabbat, B.G. and Russell, H.G. (1985), "Friction coefficient of steel on concrete or grout", *J. Struct. Eng.*, **126**(1), 1295-1303.

Richart, F.E., Brandtzaeg, A. and Brown, R.L. (1928), "A study of the failure of concrete under combined compressive stresses", University of Illinois, Urbana Champaign, **26**(12).

Saatcioglu, M. and Razvi, S.R. (1992), "Strength and ductility of confined concrete", *J. Struct. Eng.*, **118**(6), 1590-1607.

Sakino, K., Nakahara, H., Morino, S. and Nishiyama, I. (2004), "Behavior of centrally loaded concrete-filled steel-tube short columns", *J. Struct. Eng.*, **130**(2), 180-188.

Sakino, K., Tomii, M. and Watanabe, K. (1985), "Sustaining load capacity of plain concrete stub columns confined by circular steel tubes", *Proceedings of the International Specialty Confence on Concrete-Filled Steel Tubular Structures*, Harbin, China.

Sargin, M. (1971), *Stress-Strain Relationship forCconcrete and the Analysis of Structural Concrete Section*, Study No. 4, Solid Mechanics Division, University of Waterloo, Ontario, Canada.

Schmidt, M. and Fehling, E. (2005), "Ultra-high-performance concrete: Research, development and application in Europe", *ACI Struct*. *J*., **228**, 51-78.

Schneider, H. (2006), "Zum tragverhalten kurzer, umschnürter, kreisförmiger, druckglieder aus ungefasertem UHFB", Ph.D. Dissertation, University of Leipzig, Leipzig, Germany.

Schneider, S.P. (1998), "Axially loaded concrete-filled steel tubes", *J. Struct*. *Eng*., **124**(10), 1125-1138.

Setunge, S., Attard, M.M. and Darvall, P.P. (1993), "Ultimate strength of confined very high-strength concretes", *ACI Struct*. *J*., **90**(6), 632-641.

Shin, H.O., Soon, Y.S., Cook, W.D. and Michell, D. (2015), "Effect of confinement on the axial load response of Ultrahigh-strength concrete columns", *J. Struct*. *Eng*., **41**(6), 04014151-1:04014151-12.

Starossek, U., Falah, N. and Loehning, T. (2008), "Numerical analyses of the force trasfer in concrete-filled steel tube columns", *Proceedings of the 4th International Conference on Advances in Structural Engineering and Mechanics*, Jeju, Korea, May.

Susantha, K.A.S., Ge, H. and Usami, T. (2001), "Uniaxial stress-strain relationship of concrete confined by various shaped steel tubes", *Eng*. *Struct*., **23**(10), 1331-1347.

Tao, Z., Uy, B., Liao, F.Y. and Han, L.H. (2009), "Nonlinear analysis of concrete-filled square stainless steel stub columns under axial compression", *J. Constr*. *Steel Res*., **67**(11), 1719-1732.

Tao, Z., Wang, Z.B. and Yu, Q. (2013), "Finite element modelling of concrete filled steel stub columns under axial compression", *J. Constr*. *Steel Res*., **89**, 121-131.

Thai, H.T., Uy, B., Khan, M., Tao, Z. and Mashiri, F. (2014), "Numerical modelling of concrete-filled steel box columns incorporating high-strength materials", *J. Constr. Steel Res*., **102**, 256-265.

Tomii, M., Sakino, K., Watanabe, K. and Xiao, Y. (1985), "Lateral load capacity of reinforced concrete short columns confined by steel tube", *Proceedings of the International Specialty Conference on Concrete Filled Steel Tubular Structures*, Harbin, China.

Tue, N.V., Küchler, M., Schenck, G. and Jürgen, R. (2004b), "Application of UHPC filled tubes in buildings and bridges", *Proceeding of the International Symposium on Ultra High Performance Concrete*, Kassel, Germany, March.

Tue, N.V., Schneider, H., Simsch, G. and Schmidt, D. (2004a), "Bearing capacity of stub columns made of NSC, HSC and UHPC confined by a steel tube", *Proceedings of the 1st International Symposium on Ultra High Performance Concrete*, Kassel, Germany, March.

Xiao, Q.G., Teng, J.G. and Yu, T. (2010), "Behavior and modeling of confined high-strength concrete", *J. Compos*. *Constr*., **14**(3), 249-259.

Xiong, D.X. (2012), "Structural behaviour of concrete filled steel tube with high strength materials", Ph.D. Dissertation, National University of Singapore, Singapore.

Xiong, M.X., Xiong, D.X. and Liew, J.Y. (2017), "Axial performance of short concrete filled steel tubes with high-and ultra-high-strength materials", *Eng*. *Struct*., **136**, 494-510.

Yu, Q., Tao, Z., Liu, W. and Chen, Z.B. (2010), "Analysis and calculations of steel tube confined concrete (STCC) stub columns", *J. Constr*. *Steel Res*., **66**(1), 53-64.

CC